Replies to referees

Nikola Vasiljević

12^{th} July 2019

1 Referee 1

General comments

In the manuscript by Vasiljevic et al. a software library is presented which allows campaign planning for wind farm site and yield assessment with Doppler wind lidar measurements. The tool seems to be a benefit for people who have experience with lidar measurements and need an initial guess for good lidar positions in the field and for these reasons the work is technically significant and important.

Dear Referee,
We would like to thank you for your time and for your insightful comments which were used to revise and improve our manuscript. We made major changes to our manuscript. The revised manuscript follows a classical IMRAD structure and it has now been oriented on addressing research questions instead of the description of the tool. Also, we have made a change of the title from "Digitizing scanning lidar measurement campaign planning" to "Digitalization of scanning lidar measurement campaign planning", since the term 'digitalization' better suits the work we have done .Find our detailed responses below which are provided in the italic text formatting.

However there are some major concerns that can be raised with regard to its scientific significance: Experience with meteorological measurement campaigns, especially in remote locations, shows that logistical constraints are often dominating the site selection for instrument placement. The authors mention this issue, but only suggest to generate multiple layouts and select the one that is feasible in the end. In my opinion, the logistical constraints should be included in the selection process a priori, because it is a criterion for exclusion, while other criteria like the elevation angle and representative radius only increase the uncertainties which could potentially be negotiated.
We agree with the referee that as the site constraints have large impact on the final layout of measurement campaign, especially constraints in terms of access roads and power sources. We have now explicitly stated on page 5 and 6 in the reviewed manuscript that we are creating the fifth main GIS layer (aerial image

of the site) for the purpose of identifying existing road and power infrastructure. The satellite imagery is usually the first source of information a campaign planner has when he/she needs to assess whether there is necessary infrastructure for the campaign, to the very least access roads.

On page 11, line 7 - 11 in the reviewed manuscript we state that: "In practice, we would generate several layouts, and assess their feasibility by inspecting aerial images, e.g. looking for access roads and nearby power lines or houses."

To demonstrate that we followed this approach we have published the CPT outputs for the three sites in the paper.

Since the CPT is modular, one can use the tool in a reversed way, i.e., knowing in advance where you can place lidars and building towards identifying where you will be able to accurately perform measurements. This is now explicitly stated in Section 2.6 of the revised manuscript.

To my understanding the three examples for campaign planning are not actual campaigns, but generic cases. It is not shown if the defined positions would be realistic at all, neither if the tool proofed to be efficient compared to a "normal" planning by site visits and expert knowledge. The manuscript does not show if and how the tool and process improves energy yield assessment at all.
We stated in Section 3.1 of the reviewed manuscript that these are real wind farms. In the revised manuscript links to the CPT outputs for the three sites are now enclosed.

Using the CPT it takes roughly 5-15 minutes to generate a preliminary campaign layout, which otherwise will take longer if only Google Earth is used for this type of activity. The workflow and the tool does not exclude site visits, we have stated that in the reviewed manuscript (page 7 line 11 - 13). Actually, the workflow and tool should aid the process of site visit.
Also, the workflow and the tool are reducing the need for lidar expert when assessing a potential site for multi-lidar measurements.

Our manuscript is focused on facilitating the process of measurement campaign planning, and not about whether this process improves the AEP of future wind farm; we have adapted the abstract to avoid this confusion.

A great benefit would be generated if the tool allowed inexperienced users to design scanning lidar campaigns, but in multiple places in the manuscript, the authors state themselves that expert knowledge is necessary to define for example the expected range of the lidar.
The workflow and corresponding tool has been made to allow inexperienced users to design scanning lidar campaigns. Indeed, there are several input parameters which are necessary to utilize the CPT tool, specifically: represen-

tativeness radius of measurements, maximum allowed elevation angle of laser beams, minimum allowed intersecting angle between laser beams and expected lidar range. With the exception of the expected lidar range, the other three parameters have suggested values based on the existing body of knowledge. In the reviewed manuscript suggested values are stated on several locations, e.g. :

Representativeness radius: Page 3 Line 29
Maximum elevation angle: Page 2 Line 27
Minimum intersecting angle: Page 2 Line 29

We state on Page 24 Line 16 to 18 in the reviewed manuscript that we intend to extend the 'Lidar range' module to be able to perform such a task. However, this does not restrict inexperienced users of using the current version of CPT. In the revised manuscript we have provided a suggestion for the inexperienced lidar users regarding the estimation of range on Page 24 Line 17 - 21.

A part of the software that is very useful is the optimization of complex trajectories. I think this part is not presented very well. A mathematical description with a definition of the variables that are included in the optimization instead of the text-based description would be much better in my opinion. I also wonder if existing python libraries (or-tools) that are available to solve traveling salesmen problems could not be applied. What is special about this problem and what makes the developed algorithm better or more suitable than others?
Following the referee's suggestion, the revised manuscript includes an improved description of the TSP.

In general, the manuscript is very text heavy, describing simple or trivial problems in much detail while the challenging problems are not targeted. Especially the topics mentioned in section 4.2 are scientifically challenging and significant and I think that at least one of those should be tackled in a scientific paper. A topic that could be added to the list is the question of how many separate measurement points are reasonable to get a representative average wind measurement, i.e. what is the required sampling rate?
The revised manuscript has been improved in comparison to the initial submission and also the length has been reduced. The revised manuscript follows a classical IMRAD structure and it is now oriented on addressing research questions instead of the description of the tool.
The topics presented in Section 4.2, which is a subsection of Discussion, outlines our future work, and thus will be the focus of our future publications.

A major concern about the paper is that in many parts it reads more like a manual and advertisement than a scientific report and therefore could be considered inappropriate for the Wind Energy Science journal.
See our previous comment.

For all these reasons I want to encourage the authors to resubmit a manuscript that focuses on a specific research topic associated with yield assessment and lidar measurements which can be solved with that useful campaign planning tool.
We have taken into account the referee's suggestions and improved our manuscript.

Specific comments

2.1 Introduction
p.2,ll.8f: Some references should be given here. In general the introduction and manuscript are rather weak on citing relevant work.
The introduction contains citation to 14 communications related to the topic that the paper addresses. Nevertheless, we are eager to improve the introduction and therefore, we kindly ask the referee to suggest a list of references that needs to be reviewed and cited in the introduction.

2.2 Section 2
p.3,l.12: The optimal measurement positions...!?
The whole Section 2 in the revised manuscript has been rewritten.

p.3,l.29: Some references for the radius limits that are given should be provided.
We have added a references (MEASNET) to the line stating the radius limits.

p.5,ll.11-19: This seems trivial and does not need that much explanation.
The whole Section 2 in the revised manuscript has been rewritten.

p.5-6,ll.30-10: Public landcover maps can be quite erroneous and with a low resolution. The canopy heights can be particularly wrong, which would then lead to completely wrong results for possible lidar locations or unnecessary constraints.
We agree, they are however often the starting point for any resource assessment before site visits are conducted. Conservative land-cover translations, e.g. using tall tree-heights are recommended initially and the data can subsequently be corrected by the site engineers after consulting aerial imagery or conducting a site visit.

p.6,ll.29ff: Very technical and not really relevant in this context.
The whole Section 2 in the revised manuscript has been rewritten.

p.7,l.7: There are many other older and peer-reviewed references for that.
We have added the oldest reference we found when comes to the dual-radar/dual-Doppler measurements setup in the list that is Davies-Jones 1979.

2.3 Section 3
Tables 1-9: I do not think that these tables are actually necessary. The actual numbers for the measurement positions, the lidar angles etc. are irrelevant to the reader. The information that the authors want to convey should be condensed and given explicitly.Figures 2,6 and 10: It is very hard to read the small white numbers in these plots. The red circle is not visible for colorblind people on green background.
Figures 2,6 and 10: The symbols should be a bit larger and/or in better contrast to the background. *In the revised manuscript we have removed tables, nevertheless data which was in tables are now provided as a supplementary material. The commented figures have been improved.*

Technical corrections

p.1,l.1: Strange grammar in the first sentence.
The abstract has been modified.

p.1,l.2: .. wind turbine locations.
Corrected accordingly.

p.1,l.23: I do not think that 'produce' is the right word here
The sentence has been rewritten to:
The local measurements are used to produce the observed wind climate of the site.

p.2,l.10: ease of deployment
Corrected accordingly.

p.2,l.15: lays?
'lays' replaced with 'lies'

p.2,l.23: something is wrong in this sentence
The sentence has been rewritten to:
This impacts the positioning of scanning lidars since we need an unobstructed passage of the beams towards measurement points, i.e. clear line-of-sights (LOS)

2 Referee 2

General comments

The manuscript "Digitizing scanning lidar measurement campaign planning" by Vasiljevic et al. introduces and describes a planning tool for finding the optimal device position for dual-Doppler lidar setups. Though I believe that this is a very relevant tool, corresponding to a major contribution by the authors, its presentation in the manuscript is not adequate for a scientific article. In many sections the text is written rather in the style of a manual than that of a paper. I strongly recommend to rearrange the manuscript, publish some of

the contents in a manual-style technical report and focus in the paper on the research questions and the answers to these.

Dear Referee,
we would like to thank you for your time and for your insightful comments which were used to revise and improve our manuscript. The revised manuscript follows a classical IMRAD structure and it has now been oriented on addressing research questions instead of the description of the tool. Also, we have made a change of the title from "Digitizing scanning lidar measurement campaign planning" to "Digitalization of scanning lidar measurement campaign planning", since the term 'digitalization' better suits the work we have done .Find our detailed responses below which are provided in the italic text formating.

Specific comments

Page 2, line 1 – I would like to suggest to add reanalysis date here, as a quite common option for a long-term correlation.
Has been added

p. 2, l. 23 - Something wrong with the sentence "This impacts the positioning of scanning lidars can be placed..."
This sentence has been rewritten to: "This impacts the positioning of scanning lidars since we need an unobstructed passage of the beams towards measurement points. . . "

p. 3 l. 4 – The reference with the information in parentheses is too detailed here.
Details have been removed.

p. 3 ll. 8 – There should be no empty space in between two headings. Same for p. 9 ll. 26.
This is due to the LaTeX config documentclass[wes, paper]{copernicus}, which is requested to be used while paper is in the review process. If we run our LaTeX file in documentclass[wes, paper]{copernicus}, i.e. configuration once the paper is approved for publication, the blank lines dissapear.

p. 3 ll. 12 – I would suggest to refer to the respective subsections within this listing.
The whole Section 2 in the revised manuscript has been rewritten.

p. 3 l. 17 – I think for a scientific paper it is not relevant that the algorithms have been developed in Python. (This really sounds as in a manual. . .)
It is important to point out that it is developed in Python, since Python is open source, and thus to use the CPT there is no investment needed (which would be the case if the tool was developed in MatLab for instance).

p. 3 l. 17 – Here it should be briefly specified what kinds of "public databases"

it is referred to.
The whole Section 2 in the revised manuscript has been rewritten.

p. 3 ll. 25 – I am missing a verb in the sentence "The approach we have used to. . ."
The whole Section 2 in the revised manuscript has been rewritten.

p. 4 subsection 2.3 – It is only introduced in l. 27 that a dual-Doppler setup consists of "two scanning lidars". But already in l. 21 it is referred to "one of the two lidars". Check the order of information.
Dual-Doppler setups are introduced in page 2 line 17 in the reviewed manuscript.

p. 11 Figure 3 – I am wondering why there is so much empty space in the graphic. Is this figure really relevant, or couldn't it be combined with Figure 5.
Figure 3 has been removed in the revised manuscript

p. 12 Figure 4 – It is rather difficult to interpret these plots, amongst others because red and white is used for two different things each.
Red circles are used to indicate measurement point, where the addition of symbol x indicated that they are reachable by two measurement points.

p. 14 Table 1 and following tables – Not sure if so many details are needed for a scientific publication (I would say rather not).
In the revised manuscript we have removed tables, nevertheless data which was in tables are now provided as a supplementary material.

~~Digitizing~~ Digitalization of scanning lidar measurement campaign planning

Nikola Vasiljević[1], Andrea Vignaroli[1], Andreas Bechmann[1], and Rozenn Wagner[1]

[1]Technical University of Denmark - DTU Wind Energy, Frederiksborgvej 399, Building 118-VEA, 4000 Roskilde, Denmark

Correspondence: Nikola Vasiljević (niva@dtu.dk)

Abstract. ~~Multiple wind measurements is a way to reduce~~ By using multiple wind measurements when planing wind farm sites it is possible to decrease the uncertainty of wind farm energy yield assessments ~~by reducing~~ since the extrapolation distance between measurements and wind turbines locations are reduced. A WindScanner system consisting of two synchronized scanning lidar potentially represents a cost-effective solution for multi-point measurements, especially in complex terrain. However, the system limitations and limitations imposed by the wind farm site are detrimental to the installation of scanning lidars and the number and location of the measurement positions. To simplify the process of finding suitable measurement positions and associated installation locations for the WindScanner system we have devised a campaign planning workflow. The workflow consists of four phases. In the first phase, based on a preliminary wind farm layout, we generate optimum measurement positions using a greedy algorithm and a measurement 'representative radius'. In the second phase, we create several Geographical Information System (GIS) layers of information such as exclusion zones, line-of-sight (LOS) blockage, and lidar range maps. These GIS layers are then used in the third phase to find optimum positions of the WindScanners with respect to the measurement positions considering the WindScanner measurement uncertainty and logistical constraints. In the fourth phase, we optimize and generate a trajectory through the measurement positions by applying the traveling salesman problem (TSP) on these positions. The above-described workflow has been ~~digitized~~ digitalized into the so-called Campaign Planning Tool (CPT) currently provided as a Python library which allows users an effective way to plan measurement campaigns with WindScanner systems. In this study, the CPT has been tested on three different sites characterized by different terrain complexity and wind farm dimensions and layouts. The CPT ~~has shown~~ shows instantly whether the whole site can be covered by one system or not.

Copyright statement. CC BY 4.0

1 Introduction

The development of a wind farm project begins with an assessment of the wind resources and the energy yield for the planned wind farm. Best practices recommend estimating wind resources based on local wind measurements (MEASNET, 2016). Measurement campaigns designed for wind resource assessment have historically relied on anemometers and wind vanes mounted on tall meteorological masts with the goal to measure a wind climate similar to the wind climate the wind turbines

will experience during their lifetime. The local measurements are used to produce the observed wind climate of the site. To account for the seasonal and inter-annual variations of the wind the observed wind climate is long-term corrected using long-term reference data from a nearby meteorological station~~or a mesoscale model~~ , reanalysis data or meso-scale models (Carta et al., 2013). The long-term corrected wind climate is then extrapolated vertically and horizontally, typically using a flow model such as WAsP (Mortensen et al., 2014) to estimate the wind resource at hub height for every wind turbine location.

The single mast approach is affordable but can cause large uncertainties. Specifically, in complex terrain (mountainous and forested areas), the spatial extrapolation becomes challenging as the topography can significantly influence the flow. The ideal scenario would be to measure the local wind climate at every planned wind turbine position. However, erecting as many masts as wind turbines would be extremely costly and in some areas impossible.

~~Some~~ Many large wind farm projects in complex terrain ~~have been~~ are developed using multiple masts. Combining one fixed mast and one or several roaming profiling lidars moved to different positions during the campaign is another option. The advantage of roaming vertical profiling lidars lies in their ability to provide affordable high altitude measurements, ~~easiness~~ ease of deployment and absence of building-permits in comparison to the masts, while data availability and inaccuracy in complex terrain (Bingöl et al., 2009) are some of their disadvantages. However, any roaming setup brings a trade-off between the number of measurement positions and the measurement duration at each location since short measurements (e.g. of 3 months) can lead to erroneous wind climate (Langreder and Mercan, 2016).

A potential solution for multi-point measurements for wind resource assessment ~~lays~~ lies in the application of scanning lidars (Krishnamurthy et al., 2013). With a measurement range of several kilometers and a beam that can be oriented freely in any direction (Vasiljevic et al., 2016), many measurement positions can be reached without moving the hardware. Especially dual-Doppler setups (i.e., two scanning lidars) can provide accurate retrieval of horizontal wind speed and wind direction (i.e., two dimensional (2D) wind vector) at many possible positions (Vasiljević et al., 2017). While scanning lidars provide a broad range of benefits, there are also clear challenges when designing multi-lidar measurement campaigns.

Constraints which arise from scanning lidars, atmosphere and site characteristics dictate the design process mentioned above. Indeed, the beam of scanning lidars can be steered freely, but on the other hand, it can be blocked in some directions by the terrain, vegetation or other obstacles (e.g., power lines). This impacts the positioning of scanning lidars ~~can be placed such that there is a clear line-of-sight (LOS), i.e. unblocked~~ since we need an unobstructed passage of the beams towards measurement points~~.~~ , i.e. clear line-of-sights (LOS). On the other hand, the lidar characteristics (e.g., laser wavelength and output power) in combination with the atmosphere characteristics (e.g., aerosol extinction, backscatter coefficient, and atmospheric attenuation) impact the maximum expected range of the lidar. Furthermore, retrieving the 2D wind vector requires a limited beam elevation angle (e.g., smaller than 5° suggested by Vasiljević et al. (2017)) to avoid contamination of horizontal wind components with the vertical component, finally the intersecting angle of the beams at the measurement points should be large enough (e.g., bigger than 30° suggested by Vasiljevic and Courtney (2017)) to minimise the lidar measurement uncertainty (Davies-Jones, 1979; Stawiarski et al., 2013). Overall, a campaign planner has to handle several constraints at the same time to find the best measurement locations and in accordance with them generate the best possible measurement campaign layout.

In this paper, we describe a workflow and resulting digital tool (named Campaign Planning Tool, CPT) which tackle the above-described challenges involved in the planning of scanning lidar campaigns. The workflow is based on the application of the methodology for multi-lidar experiments on wind resource assessment campaigns (Vasiljević et al., 2017), which was previously used in planning of more than 20 measurement campaigns (Vasiljevic, 2018) and especially those conveyed in the New European Wind Atlas (NEWA) project (Mann et al., 2017), such as Perdigao-2015 (Vasiljević et al., 2017) and Perdigao-2017 (Fernando et al., 2019). On the other hand, the CPT has ~~been previously~~ previously been conceptualized during the WindScanner.eu project ~~(see 'WindScanner locator' description on page 8 in Vasiljevic and Hasager, 2015)~~ (see 'WindScanner locator' in Vasiljevic and Hasager, 2015).

The paper is organized as follows. Section 2 describes the workflow and corresponding elements of CPT. In Section 3 we present results of applying CPT for planning campaigns at three sites. We discuss the results and future work in Section 4, while we provide our concluding remarks in Section 5.

2 ~~Campaign planning workflow~~Methodology

2.1 Overview

~~As a starting point,~~ We assume that the location and the layout of the wind farm are ~~assumed to be known. The~~ known. These initial information are inputs to the campaign planning workflow which consists of four ~~phases which are~~ sequential phases graphically represented in Figure 1~~: The~~ . First of all, the measurement positions are ~~determined~~ optimized based on the wind farm layout. ~~The~~ Afterwards, the measurement positions are used in combination with lidar and site ~~(geographical) constraints are collected and combined. The~~ constraints to generate the map that highlights best lidar installation locations. In the next phase, the positions of the scanning lidars are determined ~~. The~~ by minimizing a dual-Doppler measurement uncertainty of horizontal wind speed while identifying existing road and power infrastructure. Finally, considering the measurement positions and positions of scanning lidars the trajectory of the laser beams through all the reachable measurement points is ~~generated~~optimized and afterwards generated. In the sections that follow each phase will be described in details followed by a short summary how the entire workflow has been digitalized and thus converted into the CPT. ~~Each phase consists of several interconnected modules (represented as icons in Figure 1). The modules entail algorithms that have been developed in Python. Data used as inputs from modules are obtained though connections to public databases. A detailed description of the different phases and associated modules are given in the following paragraphs.~~

2.2 Phase 1 - Measurement positions optimization

~~We assume that the wind farm site has been selected and that a preliminary resource assessment and wind farm layout have been made prior to the campaign planning.~~ The wind farm layout is a required input for the campaign planning ~~. It is used to determine the measurement positions.~~ workflow. For small wind farms (either a limited number of turbines and-or a limited

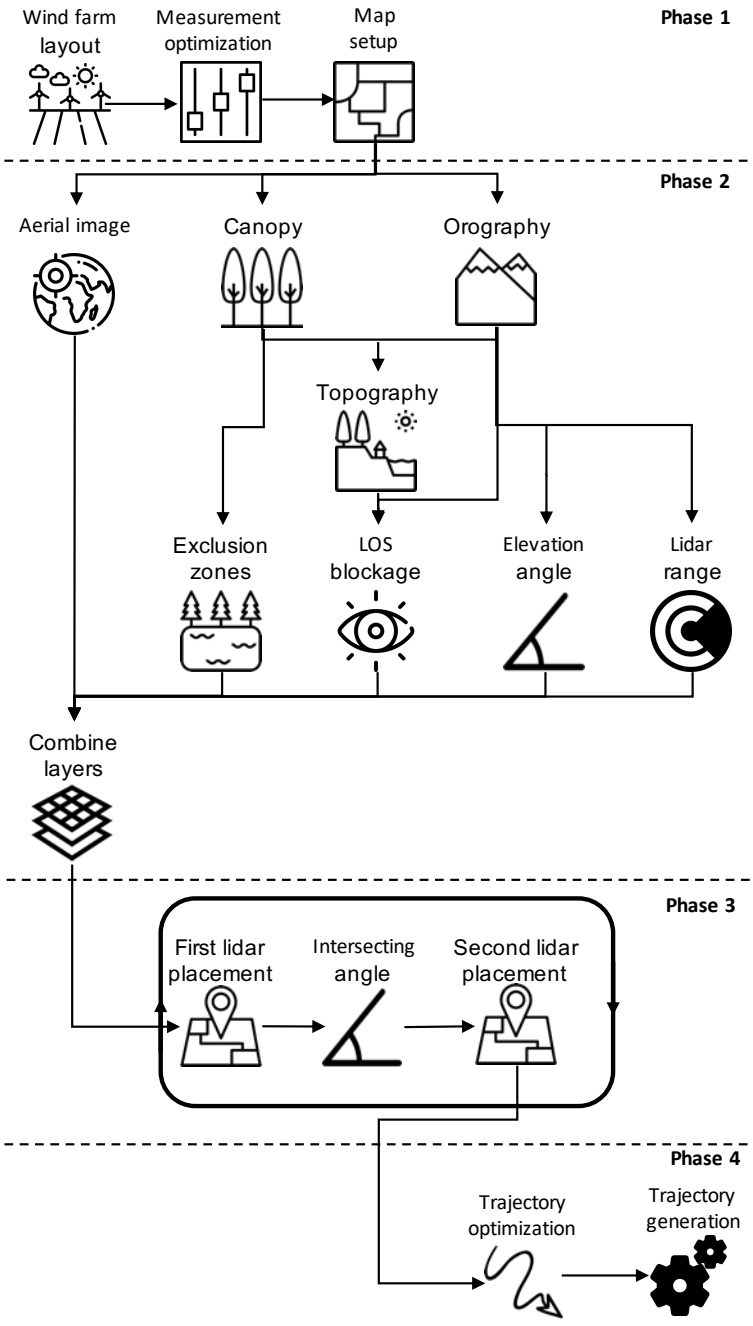

Figure 1. Campaign planning workflow (figure ~~design~~ designed using freepik.com icon database)

spatial extent) we can coincide the measurement positions with the wind turbine positions. For larger wind farms, the number of measurement points needs to be reduced.

~~The 'Measurement optimization' module optimizes the number of measurement positions and their location. The approach we have used~~ However, the reduced set of measurement points should be adequately distributed over the wind farm site to avoid long wind resource extrapolation distances. The simplest approach is to group the wind turbine locations, which are close to each other in clusters, and to assign a single measurement location per cluster. MEASNET (2016) suggests that measurements from a single location represent the wind climate over a certain area described by 'representativeness radius' (R_r). R_r has different values for different terrain types. For example, in complex terrain, the radius should be smaller than 2 km as suggested by MEASNET (2016). By solving a disc covering problem (e.g., Biniaz et al., 2017), in which we aim to find a minimum number of discs with a radius equal to R_r that cover all locations of wind turbines, we cluster the wind turbines and optimize the measurement locations. ~~The 'Measurement optimization' module includes the greedy method implementation~~ As stated in Ghasemalizadeh and Razzazi (2012) there are several ways in solving disc covering problem. One of them is a greedy approach which we adapted to suite our purpose.

In our case, the greedy algorithm implementation yields the set D of m unique disks with the radius R_r covering the set T of ~~the disc covering problem and outputs optimized measurement locations,which are geolocated in Universal Transverse Mercator (UTM) coordinate system.~~ n wind turbine positions ($T = \{ T_1, T_2, ..., T_n \}$). We are solving the disc covering problem in two dimensions (2D) by omitting height coordinate (i.e., z) of turbine positions. The greedy algorithm implementation can be described in the algorithmic sense with following steps:

~~The 'Map setup' module calculates the extent of the map for the selected site and generates a mesh over the map area.The center of the map is defined as the baryeenter of the measurement locations. To calculate the relative map extent along the x- and y-axis (~~

1. Initialize the set D ($D = \emptyset$)
2. For any unique pair of wind turbine positions (there is $p = \frac{n!}{2(n-2)!}$ unique pairs) calculate a midpoint, which is considered as a potential disc center and add it to the set $M = \{ M_1, M_2, ..., M_p \}$
3. Find the elements of the set T that are covered by each element of the set M and form an additional set S which will contain these information. To do this, calculate the distance between each element of the two sets:

$$d_{i,j} = \|M_i - T_j\| = \sqrt{(x_{M_i} - x_{T_j})^2 + (y_{M_i} - y_{T_j})^2}$$
$$i = 1, ..., p \quad \wedge \quad j = 1, ..., n \tag{1}$$

where x_m, y_m, x_t and y_t are coordinates of disc centers and turbine positions, and compare $d_{i,j}$ to R_r ($d_{i,j} <= R_r$ condition must be satisfied for a disc M_i to cover a point T_j). Through the comparisons the set S is formed. The elements of S are actually sets themselves containing wind turbine positions covered by each disc from the set M. If for example, a disc M_k covers turbine positions T_1, T_2 and T_n (i.e., ~~Easting and Northing) the sum of the distance of the~~

~~barycenter to the furthest measurement point and maximum expected range of the lidar (defined in the "Lidar Range" module)is multiplied by two. This extent is added or subtracted from the x- and y- coordinates of the barycenter, yielding four corners of the map that describes a rectangle that encompasses the wind farm site.~~ $d_{k,1}$, $d_{k,2}$ and $d_{k,n}$ are smaller or equal to R_r) the corresponding element of the set S, that is S_k will contain these elements (i.e., $S_k = \{ T_1, T_2 \text{ and } T_n \}$). Alternatively, if a disc M_k does not cover any turbine position the corresponding element of the set S will be an empty set (i.e., $S_k = \emptyset$).

~~The second input to the 'Map setup' module is the mesh resolution, which is used together with the four calculated corners to generate a mesh over the map area. Usually, the mesh resolution is set~~

4. Select a disc from the set M which covers the maximum number of points of the set T (this process is aided using the set S). Let this disc be M_i.

5. The disc M_i is added to ~~100 m to match the resolution of public databases used in Phase 2. Afterward, another copy of the map corners and~~ D and removed from M:

$$D = D \cup M_i \tag{2}$$

$$M = M \cap M_i \tag{3}$$

$$S = S \cap S_i \tag{4}$$

6. Points covered by M_i provided in S_i are removed from the set T and from any subset of the set S:

$$T = T \cap S_i \tag{5}$$

$$\forall S_j \in S, \quad S_j = S_j \cap S_i \tag{6}$$

7. Steps 1 to 6 are repeated until either the set T or S are empty :

$$T = \emptyset \quad \vee \quad S = \emptyset \tag{7}$$

8. If T is not an empty set after Step 7, then the remaining elements are added to the ~~mesh is made by re-projecting the UTM values to the latitude and longitude.~~ set D :

$$D = D \cup T \tag{8}$$

~~The outputs of Phase 1 of the campaign planning workflow are two sets of four corners describing the map area, the mesh containing~~

At the end of this process elements of the set D, that is measurement points, contain only x and y coordinates. Using the digital elevation model (DEM) from the Shuttle Radar Topography Mission (SRTM, Farr et al. (2007)) we can attach the height

information to the elements of the set D. It is important to additionally add the hub height of future wind turbines to these height information. As the last step of the first phase we generate a mesh of equally spaced points ~~covering the map area and the positions of the measurement points in the UTM coordinate system and latitude-longitude coordinate system. The UTM coordinate system is used in most modules since it is more intuitive to operate with a Cartesian coordinate system,whereas the latitude-longitude coordinate system is primarily used to fetch data from public databases containing geographical data~~over the site with the measurement point in the mesh center (see Figure 2). Lets denote the mesh as G and treat it as a set of elements $G_{i,j}$ ($G_{i,j} = \{ x_i, y_j \}$, where i=j=1, ..., l). The mesh resolution should be equal to the land cover and terrain data resolution which will be used in the second phase (typically $|x_2 - x_1| = |y_2 - y_1|$ =100 m). This avoids any interpolation of the land cover or topography datasets to our mesh.

2.3 Phase 2 - ~~Geographical and~~ Highlighting best lidar ~~related constraints~~installation locations

~~Each mesh point is considered as a potential location to place one of the two lidars. The purpose of Phase 2 is to create a map indicating a number of measurement positions that can be reached by the lidars, for each mesh point, considering~~ In this phase we will create a Geographical Information System (GIS) layer which includes site and lidar constraints while highlighting the best lidar installation locations. We will denote this GIS layer as the combined layer and treat it as a set Cl containing elements $Cl_{i,j}$. To create this layer, first we acquire land cover data, orthography data and aerial image corresponding to the extent of the previously generated mesh (Figure 2). For land cover data we can use CORINE Land Cover dataset. In case of the orography, the previously mentioned SRTM DEM datasets serves this purpose, while for the aerial image we can use the Google map server. All three data sources are publicly available. The acquired stack of data will be a base material for the combined layer creation.

At present we consider 5 types of constraints which are detrimental for a lidar installation: zones where a lidar cannot be installed (e.g., lakes~~);~~ , forests, etc.); topographical features that can block the beam; keeping the lidar elevation angle below a certain threshold to avoid measurement contamination with the vertical component of the wind; the maximum lidar range; ~~topographical features that can block the beam;~~ practical matters such as access roads.

~~The generated map extent, mesh, and measurement positions are used to create five Geographical Information System (GIS) layers, which aid the placement of the dual-Doppler setup (i.e., two scanning lidars). Three transient GIS layers need to be created first.~~

2.3.1 ~~Transient GIS layers~~

~~The "Orography" module establishes a connection to the NASA server hosting digital elevation model (DEM) data from the Shuttle Radar Topography Mission (SRTM, Farr et al. (2007)) . The DEM data have a horizontal resolution of 100 m. The map corners and mesh given as a set of latitudes and longitudes are used to acquire orography information. The Orography module fetches the elevation for each mesh point and creates an orography GIS~~ To create the combined layer which contains all the above-listed constraints, first we will generate GIS layers for each individual constraint and afterwards merge them. These

individual GIS layers are: (1) Exclusion zones layer, (2) LOS blockage layer, (3) Elevation angle layer, (4) Lidar range layer and (5) Logistical layer.

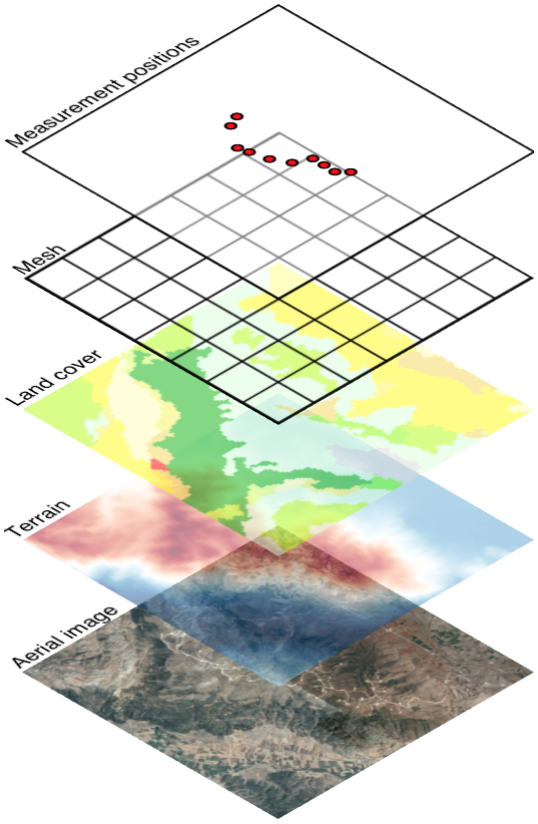

Figure 2. A stack of data used to generate the GIS layer for lidar placement: (1) measurement positions generated by solving disc covering problem, (2) mesh covering wind farm site, (3) land cover data sourced from CORINE Land Cover database, (4) terrain data sourced from SRTM DEM database and (5) aerial image sourced from the Google Map server

To create the exclusion zone layer we will use the land cover data and according to the land cover type (e.g., water surface, forest, etc.) classify areas of the site as suitable or not for a lidar installation. The ~~"Canopy" module acquires the canopy properties for the given site through the land cover information for the area. The land cover information is acquired either from the CORINE Land Cover dataset (for locations in Europe) or from the Global Land Cover 2000 dataset (for sites outside Europe). Both datasets are publicly available for download. The~~ land cover data ~~are geolocated in the UTM coordinate system; thus this module uses map corners in the UTM projection to extract a portion of~~ can be treated as a set Lc equally spaced elements $Lc_{i,j}$ containing integer values which represent so-called CLC codes that indicate the land cover ~~map.Since this transient GIS layer only contains the information on the type of~~ type (e.g., water bodies have CLC code from 40 to 44). To generate the exclusion zone layer we make a copy of the mesh (an empty mesh), walk through the mesh (going from one mesh point to another), fetch the corresponding information on land cover type from the land cover ~~, the Canopy module assigns~~

heights for each dataset, check the type and assign value of 1 or 0 to the mesh point if the land cover type based on a lookup table, which produces one more transient GIS layer (canopy height GIS layer).The look-up table is made manually.Currently, we set the look-up table such that it assigns 20 m height for areas covered by trees.

The "Topography" module creates one more transient GIS layer (topography GIS layer) by merely combining the orography and the canopy height GIS layersallows lidar installation or not (e.g., $G_{i,j} = \{x_i, y_i, 1\}$ if CLC code is equal to 12 that is 'Arable land'). An example of a fictive exclusion zone layer is shown in Figure 3.

2.3.1 Main GIS layers

The "Exclusion zones" module, using the land cover GIS layer , creates the first main GIS layer that indicates areas of the map where lidars cannot be installed (e. g., over the water surface, on the top of the forest). This GIS layer is saved as a GeoTIFF image. We use the GeoTIFF format since it supported by many GIS based software solutions, such as Google Earth or QGIS.

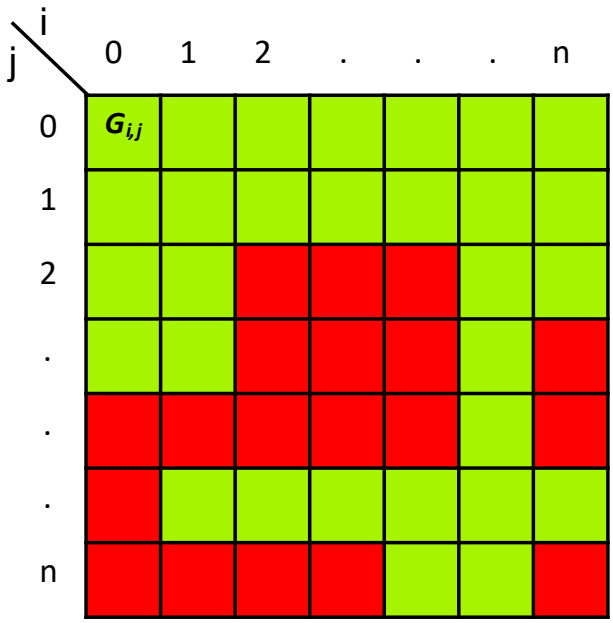

Figure 3. Fictive exclusion zone layer represented as an array: $G_{i,j}$ denotes one mesh point, red and green squares indicate bad ($G_{i,j}$ = 0) and good ($G_{i,j}$ = 1) locations for a lidar installation respectively, i corresponds to x coordinate or Easting and j corresponds to y coordinate or Northing.

The "LOS blockage" module creates the second main GIS layer. This layer is generated by performing To generate the LOS blockage layer we need to create dataset contain summed height of the terrain and canopy. To do this we will add 20 m at each location in the DEM dataset where the CORINE Land Cover dataset contains code which correspond to the forest (CLC code equal to 23, 24 and 25). Afterwards, we make a copy of the mesh, walk through the mesh, fetch the corresponding elevation from the DEM dataset, perform a viewshed analysis for measurement positions based on the topography GIS layer.Basically,

~~the LOS blockage module assigns which measurement positions~~ (Izraelevitz, 2003) from the selected mesh point to each measurement point that returns which measurement points are visible, and assign the visible measurement points to the mesh point (e.g., if measurement points D_1,D_2 and D_n are visible from ~~each mesh point.~~ $G_{i,j}$ then $G_{i,j}$ ={x_i, y_i, D_1, D_2, D_n}). In the viewshed analysis for the selected mesh point we are only taking the corresponding height from the DEM dataset (since we consider that a lidar will be installed on ground), while for the points in between the mesh and measurement points we are considering the summed height dataset. The result of this process is the LOS blockage layer which mesh points contain a set of measurement points to which there is an unobstructed LOS.

~~The "Elevation angle" module considers each mesh point as a lidar installation location and calculates the required elevation angles to steer the laser beam towards each measurement locations, based on the transient topography GIS layer. The current tool is mainly designed to plan measurements with two synchronized scanning lidars (~~As mentioned, our focus is to design a dual-Doppler ~~WindScanner system). The main goal is to~~ measurement campaign in order to retrieve the horizontal wind speed. ~~A~~ Accordingly, a low elevation beam angle is required to avoid contamination of the LOS speed measurement with the vertical component of the wind vector. ~~The module assigns which measurement positions are 'reachable' with an elevation angle below a given~~ We create the elevation angle layer to serve this purpose. This layer is created through following steps: we make a copy of the mesh, walk through each mesh point, fetch the height information from the DEM dataset, calculate the elevation angle from the mesh point to each measurement point, compare the calculated angle to a threshold value (e.g., a maximum of 5° suggested by Vasiljević et al. (2017)~~. This process creates the third GIS layer.~~ , and assign measurement points to the mesh point for which the elevation angle is below the threshold value.

~~For each mesh point , the "Lidar range " module assigns which measurement points~~ In the lidar range layer mesh points contain measurement points which are within reach of the lidar taking into account the expected range of the lidar for the given site. The ~~Lidar range module makes use of the orography transition GIS layer and positions of the measurement points (as well as their height) when performing the underlying calculations~~layer is created in a similar fashion like the previous one.

~~Finally, the fifth main GIS layeris a geolocated satellite image matching the desired area of the map (i.e., the wind farm site). The 'Satellite image' module, based on the map corners given in terms of latitudes and longitudes, compiles a list of requests for the Google map server. These requests are pushed through Google's Maps Static Application Programming Interface (API) and result in the acquisition of a set of tiles (satellite images)that cover the map area. Once all the tiles are fetched, the module assembles them in a single aerial photo of the site. Afterward, the module geolocates the aerial photo in the UTM coordinates as a GeoTIFF file. The satellite image is used in Phase 3 to identify access roads and possible power source~~To create the combined layer, we will treat the four previously derived layers as sets Ez (exclusion zone layer), Lb (LOS blockage layer), Ea (elevation angle layer) and Lr (lidar range layer). Since each set is made using the same mesh, each set contains the same number of elements. The combined layer, treated as a set Cl containing elements $Cl_{i,j}$, is derived as following:

$$Cl = \{Cl_{1,1}, Cl_{1,2}, ..., Cl_{l,l}\} \tag{9}$$

$$Cl_{i,j} = \begin{cases} \{x_i, y_j, \{\}\}, & \text{if } Ez_{i,j} = \{x_i, y_i, 0\} \\ Lb_{i,j} \cap Ea_{i,j} \cap Lr_{i,j}, & \text{if } Ez_{i,j} = \{x_i, y_i, 1\} \end{cases} \tag{10}$$

Therefore, the mesh points of the combined layer will contain which and how many measurement points are reachable considering the first four above described constraints.

Finally, the aerial image of the site (the logistical layer) is kept separate, it will serve the important purpose of identifying existing road and power infrastructure.

2.4 Phase 3 - Placement of the lidars

~~Phase 3 provides adequate locations for two scanning lidars working as a dual-Doppler system. Basically, the combination of the previous GIS layers~~ The combined layer together with underlying aerial image highlights the 'best' locations for the placement of individual lidars considering all the above-described constraints. However, designing the campaign for a dual-Doppler system, where beams from two lidars need to synchronously cross at every measurement positions, adds one more constraint: the limitation on the beams intersection angle. The measurement uncertainty of a dual-Doppler system increases when the intersecting angle between the laser beam gets small (see Vasiljevic and Courtney (2017)). Therefore the position of the second lidar is very much determined by the position of the first lidar.

~~The "Combine Layer" module provides a map indicating all possible positions for~~ Considering that we have chosen the first lidar ~~accounting for the geographical and lidar constraints described in Phase 2. The satellite image layer is used as background and we overlay the combination of the other four GIS layers as one single layer. The overlaid layer, which will be referred to as the combined layer (CB), acts as a constrainer for the lidar placement. Specifically, the CB layer is made of exclusion zones (EZ), LOS blockage (LB), elevation angle (EA) and lidar range (LR) layers.~~

~~To create the CB layer, we intersect the information from the EZ, LB, EA and LR layers at each mesh point. For each mesh point, layer LB, EA, and LR contain either an empty set or a set containing IDs of reachable measurement points. For each mesh point, the EZ layer contains a single value indicating whether it is possible or not to install a lidar (value equal to 1~~ location using the combined layer and ~~0 respectively). To create the CB layer, we use the followingformula:~~

$$CB(i) = \begin{cases} \{\}, & \text{if } EZ(i) = 0 \\ LB(i) \cap EA(i) \cap LR(i), & \text{otherwise} \end{cases}$$

~~where i represents an index~~ the logistical layer, now we need to calculate an additional layer to which we will refer as the intersecting angle layer. This layer is created as following: we make a copy of the mesh~~point.If $EZ(i)$ is equal to zero, for mesh point i, the produced set for CB layer is be empty; otherwise, it contains the intersection between three sets (i.e., three GIS layers).~~

~~The user needs to choose one of the possible locations for the first lidar (from the CB layer). The 'First lidar placement' module finds the mesh point ID, which corresponds to the first lidar position and fetches the IDs of the visible measurement points from the CB layer. The measurement points IDs and the first lidar positions are then supplied to the 'Intersecting angle' module.~~

~~Then, the "Intersecting angle" module considers that~~ , walk through each mesh point considering each mesh point ~~is a potential location for the second lidar placement and performs the following tasks:~~

~~Calculates the intersecting angles that~~ as a second lidar position, calculate intersecting angles between the two laser beams ~~will have at the measurement positions indicated by the IDs set generated by the First Lidar Placement module; Creates a set containing IDs of the measurement points~~ at each measurement point, and add those measurement points to the mesh point for which the intersecting angle is ~~higher~~ bigger than a specific value (e.g., at least 30° suggested by ~~Vasiljevic and Courtney (2017)~~ ~~); Intersects the set above with the corresponding set from the CB layer; Saves the intersected set for each mesh point creating a new GIS layer to which we will refer to as the intersecting angle (IA) GIS layer.~~

~~In this way, the IA layer highlights the~~ (Davies-Jones, 1979; Vasiljevic and Courtney, 2017)). Lets treat this GIS layer as a set Ia with elements $Ia_{i,j}$. To highlight the best locations for the ~~placement of the second lidar containing, besides the preliminary set of constraints, the constraint on the measurement uncertainty (indirectly via the intersecting angle threshold). This new GIS layer aids the campaign planner in selecting the location for the second lidar. Once the position of the second lidar is chosen the process of generating a potential lidar installation layout is completed. The output of the module 'Second lidar placement' are the positions of the two lidars and IDs of measurement points, which are 'measurable',~~ second lidar installation the intersecting angle layer should be intersected with the combined layer, i.e. ~~, visible by the two lidars considering all the constraints. :~~

~~It is important to highlight that the CB layer can provide several possible positions for the first lidar . In Phase 3, the workflow user needs to consider every possible~~

$$Sl = Cl \cap Ia \tag{11}$$

where Sl is a set corresponding to the newly created GIS layer for the second lidar placement. The process of selecting a position for the first lidar~~and can, for each of them, run the "First lidar placement" and~~ , followed with the generation of the ~~"Intersecting Angle" modules to identify the possible positions for the second lidar . For most sites, several measurement campaign layouts can be generated. It is advisable~~ layer for locating the second lidar and selection of the second lidar position should be performed several times to generate several ~~potential layouts~~potentials experiment designs, since only during a field visit ~~will it~~ it will be possible to determine the most likely design for the measurement campaign. Once the second lidar position is determined, we derive a set of reachable measurement points Dr by both lidars which is actually a subset of the set D ($Dr \in D$).

2.5 Phase 4 - Trajectory optimization and generation

The fourth phase consists of the optimization of the path through the measurement points and the generation of the corresponding trajectory.

In the previous phases, we derived the measurement locations and dual-Doppler campaign layout(s). A next task is to optimize the path through those positions such that the motion of the scanner heads required to steer the beams takes the least amount of time (i.e., increasing sampling rate). One way to achieve this is to adapt the solution for the traveling salesman problem (TSP). In the regular TSP, the goal is to find the shortest path through a set of n cities that a traveling salesman needs to visit. There are multiple approaches to solve the TSP (Reinelt, 1994). One of the simplest implementation of the TSP solution is Nearest Neighbor Heuristics (NNH). As stated in (Reinelt, 1994): *This heuristic for constructing a traveling salesman tour is near at hand. The salesman starts at some city and then visits the city nearest to the starting city. From there he visits the nearest city that was not visited so far, etc., until all cities are visited, and the salesman returns to the start.*

In our case, we have ~~two 'salesmen' (i.e., lidars), and two set of cities because the two lidars do not have identical locations. To level our problem of the trajectory optimization to the regular TSP problem we need to convert two 'salesmen' and two sets of 'cities' to a single salesman and single set of cities. To achieve this, we do the~~ a single set of measurement points D_c which needs to be simultaneously visited by the two laser beams. Since typically two scanning lidars will not be symmetrically positioned with respect to the measurement points we will have two different sets of steering angles D_{s1} and D_{s2} corresponding to the first and second lidar respectively which enable 'visiting' the measurement points with the laser beams. Therefore, we cannot directly apply the above described heuristics. The TSP NNH solution needs to be adapted.

Lets consider that the set D_c is defined as:

$$D_c = \{D_{c,1}, D_{c,2}, ..., D_{c,n}\}, D_{c,i} = \{x_i, y_i, z_i\} \tag{12}$$

while D_{s1} and D_{s2} are defined as:

$$D_{s1} = \{D_{s1,1}, D_{s1,2}, ..., D_{s1,n}\}, D_{s1,i} = \{\theta_{1,i}, \varphi_{1,i}\} \tag{13}$$

$$D_{s2} = \{D_{s2,1}, D_{s2,2}, ..., D_{s2,n}\}, D_{s2,i} = \{\theta_{2,i}, \varphi_{2,i}\} \tag{14}$$

additionally we will make a set I which will contains indexes of the sets' elements:

$$I = \{1, 2, ..., j, ..., n\} \tag{15}$$

The adapted TSP NNH solution for dual-Doppler trajectory can be described in the algorithmic sense with following steps:

1. ~~We create two arrays, one containing measurement points visible by both WindScanners, and second one corresponding to the trajectory which will be empty~~Initialize empty sets T_{l1} and T_{l2} ($T_{l1} = T_{l2} = \emptyset$), which will contain ordered elements of the optimized trajectory.

2. ~~From the measurement point array, we randomly select one of the points, add it to the trajectory array and then remove the same point from the measurement point array. At the end of this step, the trajectory array contains one measurement point.~~ Select an arbitrary index j from the set I.

3. ~~Next, we calculate the required~~ Set an element l to j ($l = j$).

4. Select elements $D_{s1,l}$ and $D_{s2,l}$.

5. Add the elements $D_{s1,l}$ and $D_{s2,l}$ to the set T_{l1} and T_{l2} respectively, and remove index j and elements $D_{s1,l}$ and $D_{s2,l}$ from the set I, D_{s1} and D_{s2} respectively:

$$T_{l1} = T_{l1} \cup D_{s1,l} \tag{16}$$

$$T_{l2} = T_{l2} \cup D_{s1,2} \tag{17}$$

$$I = I \cap j \tag{18}$$

$$D_{s1} = D_{s1} \cap D_{s1,l} \tag{19}$$

$$D_{s2} = D_{s2} \cap D_{s2,l} \tag{20}$$

6. Calculate sets $\Delta\alpha_1$ and $\Delta\alpha_2$ which contains elements $\Delta\alpha_{1,il}$ and $\Delta\alpha_{2,il}$ (i takes values from the set I), defined as:

$$\Delta\alpha_{1,il} = \{\mid \theta_{1,i} - \theta_{1,l} \mid, \mid \varphi_{1,i} - \varphi_{1,l} \mid\}$$
$$i = 1, 2, ..., n \tag{21}$$

$$\Delta\alpha_{2,il} = \{\mid \theta_{2,i} - \theta_{2,l} \mid, \mid \varphi_{2,i} - \varphi_{2,l} \mid\}$$
$$i = 1, 2, ..., n \tag{22}$$

that describe relative angular moves ~~that two lidars would need to perform from the current~~ for the two lidars from the measurement point described by the last element of the ~~trajectory array to reach any remaining measurement point in the measurement point array. This forms two arrays containing angular moves corresponding to the two lidars.~~ sets T_{l1} and T_{l2} (i.e., $D_{s1,l}$ and $D_{s2,l}$ respectively) to all remaining measurement points described by elements of D_{s1} and D_{s2}.

7. ~~In the next step, we form a new array containing the maximum value for the pairs of the angular moves from the two above-described arrays. This step converts our problem of optimizing the path through the measurement points to the general TSP problem, since now we have single set of cities and single traveling salesman.~~ Form a set B containing maximum concurring elements of the sets $\Delta\alpha_1$ and $\Delta\alpha_2$:

$$B = \{max(\Delta\alpha_{1,1l}, \Delta\alpha_{2,1l}), max(\Delta\alpha_{1,2l}, \Delta\alpha_{2,2l}), ...,$$
$$max(\Delta\alpha_{1,1n}, \Delta\alpha_{2,1n})\} \tag{23}$$

8. ~~Next, we find the element which has minimum valuein the maximum angular move array based. The corresponding measurement point for this element represents the next trajectory point, which is then added to the trajectory array and removed from the measurement point array.~~ Find index j of an element of the set B which has lowest value.

9. ~~We repeat~~ Repeat steps 3 to ~~5 until the measurement point list is empty~~ 8 until the sets D_{s1} and D_{s2} are empty (D_{s1}=D_{s2}=$\emptyset$).

The ~~above-described steps are encapsulated as an algorithm, which is a fundamental block of the 'Trajectory optimization' module. The output of the module is an efficient order to probe the measurement points in space with the two laser beams steered by the lidar scanner heads~~main modifications of a standard TSP NNH solution is the addition of Step 7 which secures that the trajectory will be optimal for both lidars instead of only one. The difference between the standard and adapted TSP NNH solution can seen from an example shown in Figure 4.

To get the lidars to actually follow the optimized trajectory, we need to describe the motion of the scanners as a function of time. In other words, we need to 'attach' the time component of the trajectory to the spatial description we yielded in the previous steps. ~~We aim at minimizing the time required to move from one measurement point to another. Since we derived the order of measurement points to do this, we need to know the kinematic limits of the scanner heads, specifically maximum speed and maximum acceleration. These two parameters along with the required angular move that the scanner head of each lidar needs to do to steer the laser beams from one to another measurement point are used to solve the kinematics elevator problem (e.g., Al-Sharif, 2014). The solution for this problem yields the minimum required time to move a scanner head from one to another position. Since we have two lidars that move to a measurement point, we will generally have two different moving times. To keep the lidar measurements in sync in both time and space, we take the maximum of the two derived values.~~ When calculating the timing for the trajectory, we assume that the lidars will stop at each measurement point and sample wind speed before they continue to the next measurement points. Therefore, we expect that lidars will perform so-called step-stare trajectories. There are several reasons for selecting step-stare trajectories instead of continuously scanning the flow through the trajectory described by the measurement points. The most important reason is that the current commercial scanning lidars allow only step-stare implementation of complex trajectories. ~~Furthermore, the application of the continuously scanning through complex trajectories is not trivial and , it requires more complex kinematic models than the one described by the elevator problem.~~ Also, the timing for the step-stare scans can be calculated using a simple solution for Kinematics Elevator Problem (KEP) (e.g., Al-Sharif, 2014) considering an infinite jerk:

$$T_{move} = 2 * \sqrt{\frac{\Delta\beta}{A_{max}}} \tag{24}$$

where T_{move} is a minimum time required to perform an angular motion $\Delta\beta$ considering a maximum allowed acceleration of the lidar scanner head A_{max}.

Since we have two lidars that move to from one to another measurement point, we will generally have two different moving times to perform angular motions. To keep the lidar measurements in sync we take the maximum of the two derived values.

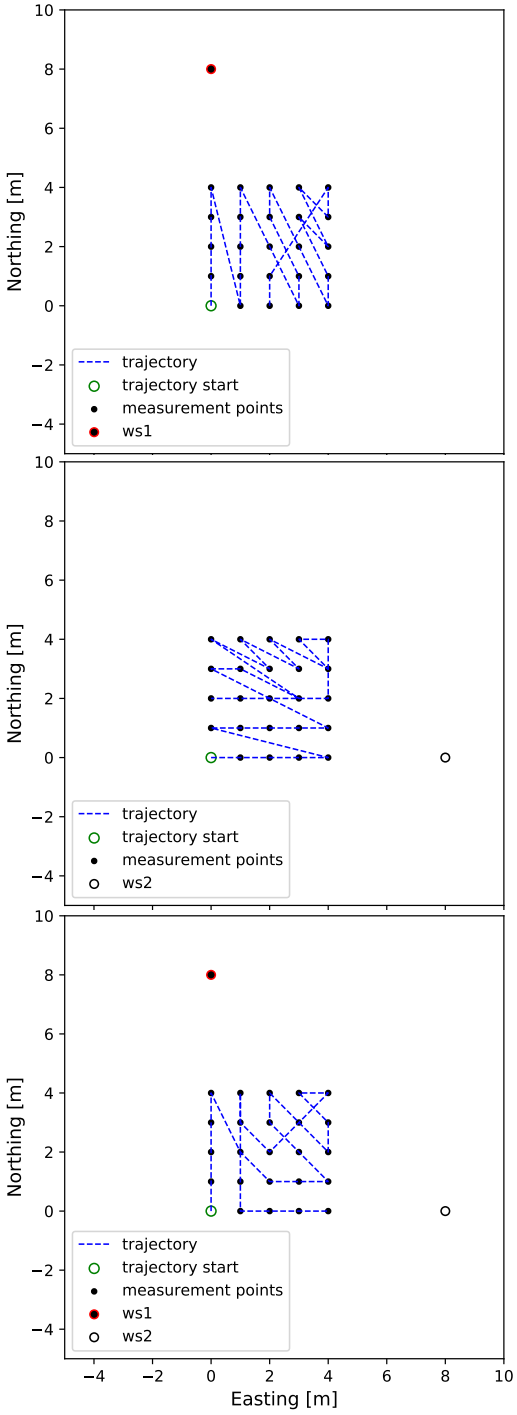

Figure 4. TSP NNH: top image - standard TSP NNH for lidar $ws1$, mid image - standard TSP NNH for lidar $ws2$, bottom image - adapted TSP NNH for two lidars $ws1$ and $ws2$

2.6 Campaign planning tool

The previously described workflow has been digitalized resulting in the Campaign Planning Tool (CPT). The CPT is developed in Python in order to be an open source solution which does not require commercial products to be used, improved and further developed. The tool is modular allowing end users to build their own workflows. For example, considering that the installation locations of lidars are predetermined one can recombine modules to find where measurements can be taken followed with the trajectory optimization and generation. At time of writing this manuscript, the tool contains 16 modules where each module is depicted as an icon in Figure 1. Currently, a public release of the tool on a dedicated GitHub (https://github.com/recast-reduced-assesment-time/campaign-planning-tool) is scheduled for the autumn 2019.

3 ~~Campaign planning workflow in action~~Results

3.1 Overview

In this section, the campaign planning workflow is demonstrated through the application of CPT on three different wind farm sites, which are named by their country of origin: Scotland (Vasiljevic and Bechmann, 2019a), Italy (Vasiljevic and Bechmann, 2019b) and Turkey (Vasiljevic and Bechmann, 2019c). The only information needed for each site is the wind turbine positions and their hub height. This input could be generated arbitrarily, but to make the examples realistic actual operating wind farms have been chosen. ~~The three selected sites are all located in complex terrain, where large spatial variations in wind speed are expected, and the sites are thus relevant for scanning lidar campaigns. The spatial extent of the sites varies greatly: with a single centrally placed met mast the maximum distance to a turbine would be 1 km, 4 km and 5 km for the three sites. Since only the wind farm layout and the turbine hub height are needed for the demonstration, any other details that could identify the wind farms are omitted in the descriptions below. The wind farms are just named by their country of origin: Scotland, Turkey, and Italy.~~

For all three sites, we aim to design the campaign for the long-range WindScanner system configured in a dual-Doppler mode (i.e., the system will have two scanning lidars). The system is described in details in Vasiljevic et al. (2016). To demonstrate the workflow, the most essential bits of information is the maximum range of the lidars, which is 6 km, and maximum ~~velocity and~~ acceleration of the scanner heads, which ~~are 50°/s and~~ is 100°/s^2~~respectively.~~. Results which will be described in the following sections are accessible as a data collection (Vasiljevic et al., 2019) or as an individual datasets (Vasiljevic and Bechmann, 2019a, b, c).

3.2 Site 1 - Scotland

The Scottish site consists of 22 wind turbines with 47-m hub-heights and has a quite compact layout (Figure 5). The distance between adjacent turbines is about 300 m (5 rotor diameters). The wind farm is placed on a 300-m tall hill surrounded by rolling hills of farmland with windbreaks and patches of forest. The hill is quite steep with maximum slopes of 20% from the main south-western wind direction. The site is located 17 km from the coast and can, therefore, be considered an inland site.

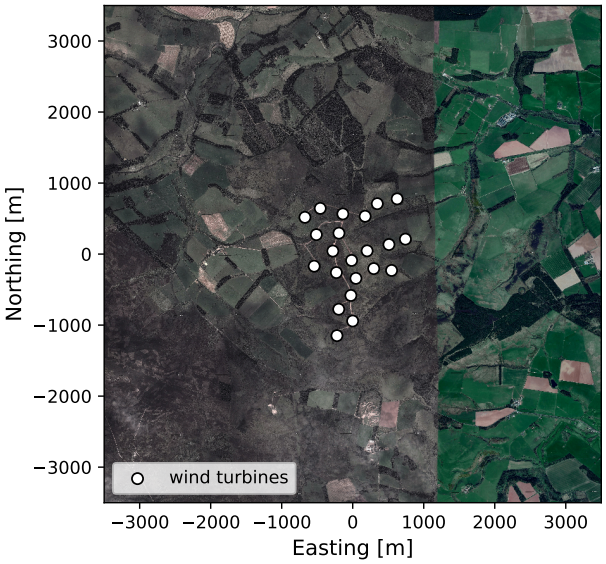

Figure 5. ~~Google Earth~~ The aerial image of the Scottish site~~. A 1 km radius circle illustrates the extent of the wind farm~~

Due to the compact design of the wind farm, we decided to skip the measurement position optimization and try to generate a measurement campaign in which we intend to measure at every wind turbine position. ~~Figure ?? shows the map extent and locations of the wind turbines, now measurement positions, generated by the 'Map Setup' module.~~ Considering that the site is relatively close to the coast, surrounded by agricultural land, and the altitude is about 300 m above sea level (asl.), thus relatively low, the site should experience a good concentration of aerosols. Nevertheless, we cannot expect that the WindScanners will have 6 km range all the time and assume that on average the WindScanners would have a range of at least 3 km at the selected site (i.e., a half of the maximum claimed range). This estimation is based on our experience in doing measurement campaigns at various locations and in different atmospheric conditions.

Using this range together with the map extent, ~~we generated the CB~~ the CPT tool outputs the combined layer (see top image in Figure 6). The dark red color areas show positions from where an individual scanning lidar can reach out to all measurement positions. Those areas are relatively large because the wind farm layout is compact. For the purpose of this example, we chose to place the first WindScanner at the South of the wind farm (coordinates of 100 m, -1600m and ~~350~~ 400 m in Easting, Northing and altitude asl. respectively relative to the map center coordinates of 535662 m, 6183892 m in Easting and Northing, UTM zone 30 U).

~~Measurement locations for Scottish site: black dots - wind turbine positions that also correspond to measurement positions.~~

As explained in Section 2 (Phase 3), the first lidar placement is ~~detrimental~~ instrumental for the second lidar placement because of the intersecting angle between the respective lidars' beams. There is only one area of the map where the placement of the second lidar assures that all measurement points are within reach and measurable with fair accuracy (bottom image in Figure 6). By selecting the position of the second lidar (coordinates of 1600 m, ~~600m~~ 400 m and 318 m in Easting, Northing and

altitude asl. respectively relative to the map center coordinates), we complete the generation of one measurement campaign layout. In practice, we would generate several layouts (for different positions of WindScanner 1 and WindScanner 2), and assess their feasibility by inspecting aerial images, e.g. looking for access roads and nearby power lines or houses. However, for the sake of demonstrating the workflow, we have generated only a single layout.

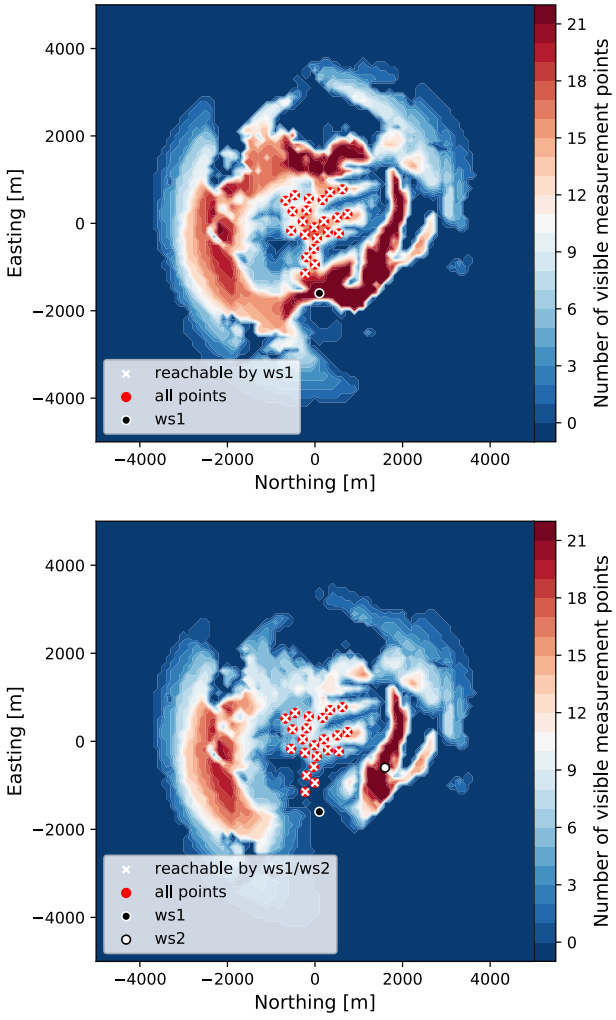

Figure 6. Placing lidars at the Scottish site: top image - locating first lidat at the ~~CB~~ combined layer, bottom image - locating second lidar at ~~IA~~ the second lidar placement layer

Since we have both the measurement and lidar positions, we have all the elements to optimize and generate the trajectory. Figure 7 shows the optimum trajectory through the measurement points, resulting from the modified TSP (see Section 2 - Phase 4). ~~The second column of Table ?? and Table ?? show the trajectory order and angular positions respectively.~~

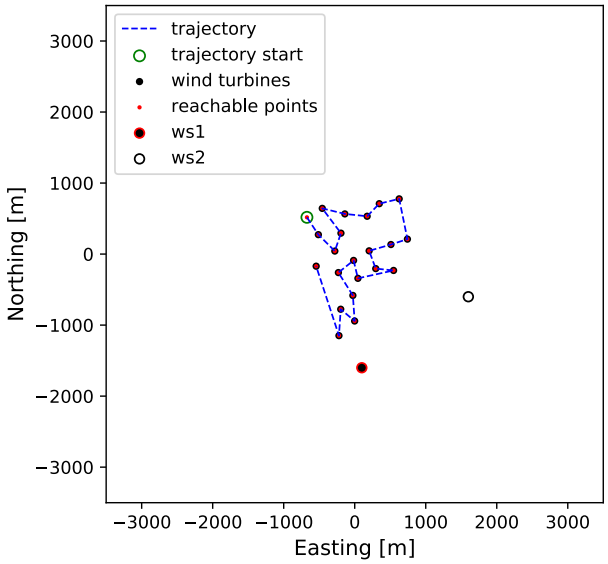

Figure 7. Final campaign design at Scottish site

Considering the kinematic limits of the scanner head and that we are performing step-stare scans, we can apply the elevator kinematic problem on the trajectory points~~(Table ??)~~. This step yields the required time to move the scanner heads from one point of the trajectory to another~~. The input to the elevator kinematic problem is the foreseen angular displacement, maximum velocity, and acceleration of the scanner head. In our case , we have two angular movements for each measurement point (see Table ?? and ??) since the scanner heads will move in both azimuth and elevation axis since the measurement points do not lay on the same altitude. However, the displacement in the azimuth angle θ is much larger than the one in the elevation angle φ, and it will dictate the minimum time for the scanner head motion (see Table ??). Therefore, we use the displacement in the azimuth angle as an input for the kinematic model (see the second and third column in Table ??). The kinematic model calculates the minimum time to perform the move (see the third and fifth column in Table ??). As we can see in Table ?? the minimum time for each WindScanner will be different. To keep the WindScanners synchronized, we use the maximum of the two calculated values for each trajectory point (last column in Table ??). At each point in the trajectory, the WindScanners will accumulate spectra over a period of 1 s. Therefore,~~ , which in our case is about 14 s for the entire trajectory with additional 22 s for measurements (consult table in Vasiljevic and Bechmann (2019a)). Overall, one complete scan of all measurement points will take about 36 s, ~~of which 22 s is for measurements while the remaining amount is for the motion between the measurement points, which~~ which results in about 16 samples of each measurement point per 10-min period. Typically we aim at having at least ten samples per 10-min period which is satisfied with this configuration.

~~Measurement points at the Scottish site. All position values rounded to two decimals. Initial order Trajectory order Easting mNorthing mHeight mVisible by WS1 Visible by WS2 1 1 -673.0 517.5 323.0 True True2 5 -457.0 643.5 321.0 True True3 6 -139.0 565.5 335.0 True True4 7 175.0 532.5 346.0 True True5 8 346.0 709.5 341.0 True True6 9 626.0 777.5 327.0 True~~

True7 2 -512.0 273.5 338.0 True True8 4 -194.0 294.5 358.0 True True9 22 -543.0 -170.5 347.0 True True10 3 -280.0 42.5 370.0 True True11 16 -16.0 -89.5 383.0 True True12 12 203.0 45.5 372.0 True True13 11 510.0 134.5 349.0 True True14 10 742.0 210.5 335.0 True True15 20 -197.0 -776.5 352.0 True True16 17 -230.0 -260.5 380.0 True True17 15 45.0 -341.5 383.0 True True18 13 296.0 -204.5 366.0 True True19 14 547.0 -230.5 338.0 True True20 18 -26.0 -582.5 363.0 True True21 19 -1.0 -942.5 351.0 True True22 21 -222.0 -1148.5 351.0 True True

Angular positions for WindScanners for the Scottish site. All values rounded to two decimals. Trajectory θ_{ws1} $^{\circ}\varphi_{ws1}$ $^{\circ}\theta_{ws2}$ $^{\circ}\varphi_{ws2}$ $^{\circ}$points 1 339.95 -0.69 296.19 0.112 341.91 -0.35 292.48 0.53 346.98 0.68 288.88 1.54 351.18 0.24 296.51 1.145 346.06 -0.72 301.16 0.076 353.7 -0.39 303.84 0.477 2.01 -0.11 308.49 0.888 6.08 -0.22 316.25 0.739 12.47 -0.54 324.75 0.3110 19.52 -0.45 313.39 0.8211 13.3 -0.03 303.99 1.3512 3.58 0.76 294.82 2.0113 7.99 0.65 286.89 2.0214 18.07 -0.48 289.36 1.0315 357.5 1.5 279.46 2.3616 355.61 1.25 287.55 2.217 346.17 1.25 280.53 1.9118 352.94 0.73 270.63 1.5919 351.27 0.09 257.94 1.1520 340.18 0.13 264.41 1.0821 324.53 0.1 253.26 0.9922 335.79 -0.11 281.35 0.76

Result of applying elevator kinematic problem on trajectory points for the Scottish site: step-stare order - indicate motion from one to another trajectory point ,$\Delta\theta_{ws}$ - angular displacement in azimuth angle (θ), ΔT_{ws} - minimum required time to complete the angular motion. All values rounded to two decimals.

Step-stare order $\Delta\theta_{ws1}$ $^{\circ}\Delta T_{ws1}$ ms$\Delta\theta_{ws2}$ $^{\circ}\Delta T_{ws2}[ms]$ Max(ΔT_{ws1},ΔT_{ws2}) ms1->2 1.96 280 3.71 385 3852->3 5.06 450 3.60 379 4503->4 4.20 410 7.63 552 5524->5 5.12 453 4.65 431 4535->6 7.64 553 2.68 327 5536->7 8.31 577 4.65 431 5777->8 4.06 403 7.76 557 5578->9 6.39 506 8.50 583 5839->10 7.05 531 11.36 674 67410->11 6.22 499 9.39 613 61311->12 9.72 624 9.18 606 62412->13 4.41 420 7.92 563 56313->14 10.08 635 2.47 314 63514->15 20.57 907 9.9 629 90715->16 1.89 275 8.09 569 56916->17 9.44 614 7.02 530 61417->18 6.78 521 9.89 629 62918->19 1.67 258 12.69 712 71219->20 11.09 666 6.46 508 66620->21 15.64 791 11.15 668 79121->22 11.25 671 28.09 1110 111022->1 4.16 408 14.84 770 770

3.3 Site 2 - Italy

The Italian wind farm consists of 36 wind turbines with a 78-m hub-height. The turbines are distributed over a large area (see Figure 8) but somehow clustered in small groups (Figure 13) often with inter-turbine distances of less than 300 m (3 rotor diameters). With a coastline only 10 km to the West, a complex coastal-inland wind climate transition is expected to occur across the wind farm. The terrain has an average 7% slope from the coast to the wind farm. The wind farm is surrounded by farmland, though in a range of about 7 km there are several medium-size towns forming an urban area ring around the farm site.

Given the specific layout of the wind farm, having more or less isolated groups of tightly packed wind turbines, we decided to apply the measurement point optimization. For this wind farm, the representativeness radius was set to 500 m, which is four times smaller than the value suggested for the complex terrain sites (MEASNET, 2016). With this conservative setting, the optimization routine found 13 discs of radius equal to 500 m which covers all 36 wind turbine locations (Figure 13). The disc centers are measurement positions. The disc centers coordinates are listed in Table **??**.

From there, the workflow was applied in the same way as it was for the Scottish site. In comparison to the Scottish site, the Italian wind farm is even closer to the sea, and it is surrounded by an urban area that in our experience increases the

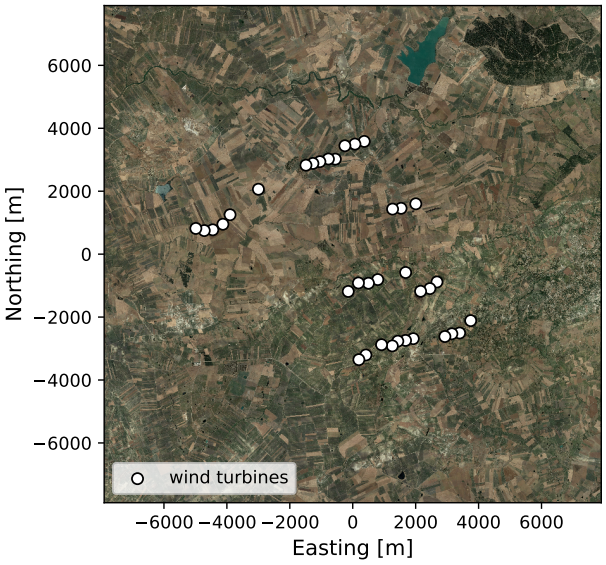

Figure 8. The aerial image of the Italian site~~(source Google Earth). A 5 km radius circle illustrates the large extent of the wind farm~~

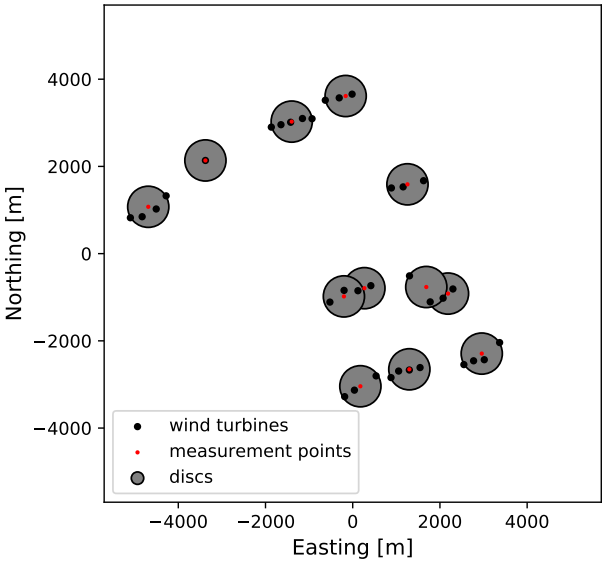

Figure 9. Measurement locations for Italian site: black dots - wind turbine positions, red circles - discs covering wind turbine positions, green dots - optimized measurement positions (i.e., discs' centers)

aerosol concentration resulting in an improved lidar range. Therefore, for the Italian site, we can expect to have an average measurement range of 4 km for the WindScanners. The ~~CB~~ combined layer generated by the CPT is shown as the top image in Figure 10. For this site, there are actually no positions from which ~~a~~ any lidar can reach all 13 measurement positions~~(in spite of the 4 km assumed measurement range and the reduced number of measurement points)~~. At best, there are only two locations from which one lidar can reach 11 out of 13 measurement points. The top image of Figure 10 shows the selected location for the first lidar installation (coordinates of -910 m, -640 m and 227 m Northing, Easting and height asl. respectively relative to the map center coordinates of 297200 m and 4189966 in Northing and Easting respectively, UTM zone 33 S).

The ~~IA layer~~ layer for the second lidar placement (the bottom image in Figure 10) shows that the second lidar can only reach 7 measurement positions at most and this can only be achieved from a few locations. Of these locations, we selected one which assures that we cover the largest extent of the wind farm~~. In other words, instead of measuring at positions which correspond to closely located wind turbine clusters we probe the wind resources across nearly the entire site and thus getting better~~ , thus getting good spatial information on the farm wind resources. The coordinates of a selected location for the second lidar are 1600 m, 110 m and 278 m in Northing, Easting and height asl. relative to the map center coordinates (the bottom image in Figure 10).

Considering the positions of WindScanners, reachable measurement points, and kinematic limits, we derived an optimum trajectory through the measurement points and calculated the timing for the synchronized scanner head motions (~~see Figure 11and Table ?? - ??~~Figure 11). Based on the calculated timing for the scanner heads motion and considering one second accumulation time per measurement point, one scan through all the points takes roughly 21 s of which 7 s are spent on measurements (consult table in Vasiljevic and Bechmann (2019b)). This provides us with about 28 measurement samples at each measurement point within a 10-min period.

~~Measurement points at the Italian site. All position values rounded to two decimals. Initial order Trajectory order Easting mNorthing mHeight mVisible by WS1 Visible by WS2 1 1 -1019.32 2953.88 384.0 True True2 3338.73 -2365.62 336.0 False False3 5 1678.28 -2726.12 357.0 True True4 -4308.87 1000.38 229.0 True False5 -4556.37 883.38 243.0 True False6 7 2564.83 -989.62 407.0 True True7 2066.98 -839.12 381.0 True False8 2 1635.38 1515.38 344.0 True True9 4 647.38 -866.12 352.0 True True10 6 555.33 -3115.12 323.0 True True11 217.83 3540.38 308.0 False True12 3 177.88 -1054.62 328.0 True True13 -2998.02 2062.88 244.0 True False~~

~~Angular positions for WindScanners for the Italian site. All values rounded to two decimals. Trajectory θ_{ws1} $^\circ\varphi_{ws1}$ $^\circ\theta_{ws2}$ $^\circ\varphi_{ws2}$ $^\circ$points 1 358.27 2.5 317.32 1.572 49.76 2.01 1.34 2.693 110.89 4.95 230.71 1.564 98.29 4.54 224.35 3.15 128.87 2.24 178.47 1.596 149.37 1.91 197.98 0.767 95.76 2.95 138.83 5.04~~

~~Result of applying elevator kinematic problem on trajectory points for the Italian site: step-stare order - indicate motion from one to another trajectory point ,$\Delta\theta_{ws}$ - angular displacement in azimuth angle (θ), ΔT_{ws} - minimum required time to complete the angular motion. All values rounded to two decimals. Trajectory order $\Delta\theta_{ws1}$ $^\circ\Delta T_{ws1}$ ms$\Delta\theta_{ws2}$ $^\circ\Delta T_{ws2}[ms]$ Max(ΔT_{ws1},ΔT_{ws2}) ms1->2 51.49 1535 44.02 1427 15352->3 61.13 1764 130.63 3136 31363->4 12.6 710 6.36 504 7104->5 30.58 1156 45.88 1455 14555->6 20.5 906 19.51 883 9066->7 53.61 1614 59.15 1688 16887->1 97.49 2475 178.49 4072 4072~~

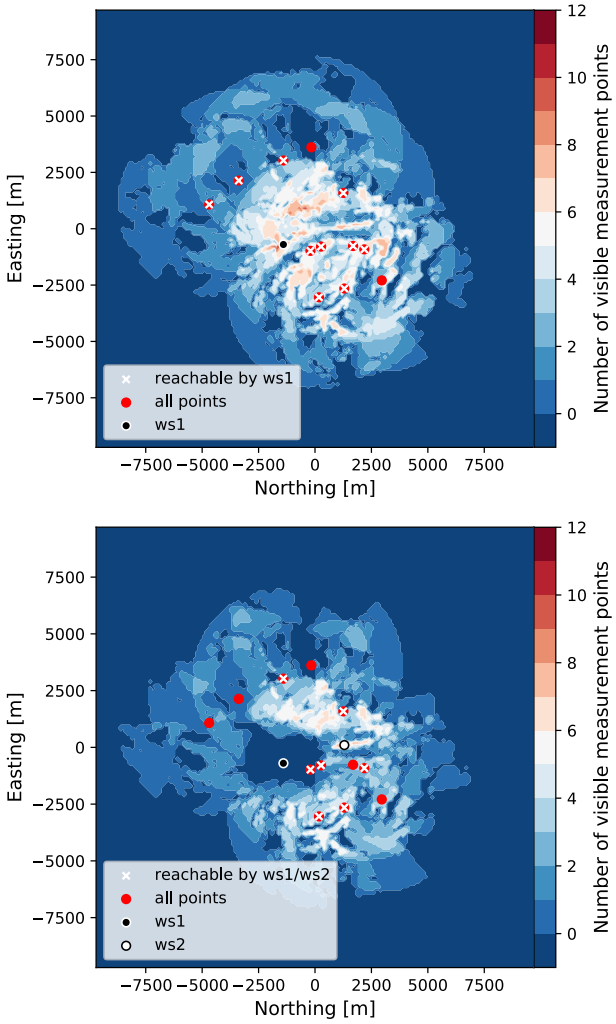

Figure 10. Placing lidars at Italian site: top image - locating first lidat at the ~~CB~~ combined layer, bottom image - locating second lidar at ~~IA~~ the second lidar placement layer

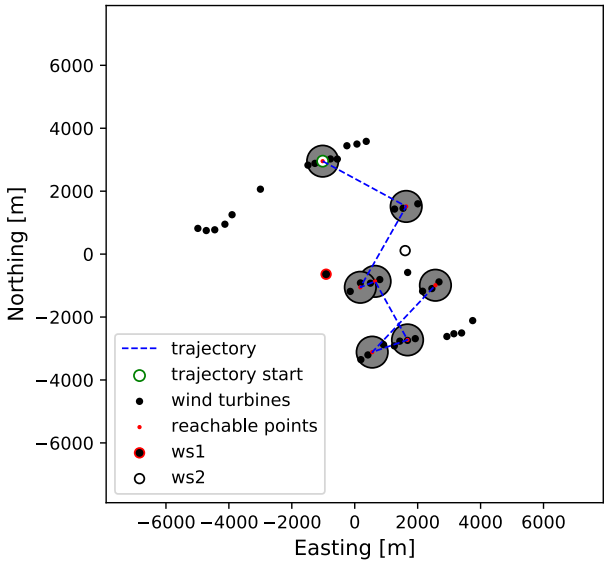

Figure 11. Final campaign design for Italian site

3.4 Site 3 - Turkey

The Turkish wind farm consists of 22 wind turbines with a 80-m hub-height. The wind farm extends 8 km from North to South (see Figure 12) with the three most northerly turbines separated by about 2 km from the rest. The inter-turbine distance is 400-500 m (4-5 rotor diameters) for most turbines. The turbines are located along a 1600 m tall North-South ridge and the main wind direction from North-East (i.e., perpendicular to the ridge line). In the main wind direction the mean terrain slopes are about 12% and with extremes reaching 50% the site should be regarded as very complex. The land cover is sparse vegetation with a patch of forest along Western facing slopes.

For this site, we assumed the average lidar measurement range to be 3 km, and we used the representativeness radius of ~~400~~ 500 m. Our assumption on the average range in case of the Turkish site is probably closer to what a lidar would probably achieve in field operation (thus less conservative) due to operation in high altitude where we usually experience low aerosol concentration and often low clouds and fog. On the other hand, the selected representative radius is 100 m lower than in the case of the Italian site, thus about 5 times smaller than the recommended value by MEASNET. Running the workflow ~~with~~ using these parameters ~~, the "Measurement optimization" module output~~ we generate a measurement layout with 10 measurement positions (see Figure 13~~and Table ??) and Phase 2 of the workflow resulted in the CB layer~~) with the associated combined layer for the first lidar placement shown in Figure 14, top image.

~~Measurement points at the Turkish site. All position values rounded to two decimals. Initial order Trajectory order Easting mNorthing mHeight mVisible by WS1 Visible by WS2 1 1276.0 -3694.0 1633.0 False False2 5 696.0 -2254.0 1676.0 True True3 556.0 -3074.0 1665.0 False False4 4 -404.0 -954.0 1613.0 True True5 3 -924.0 166.0 1610.0 True True6 816.0 4066.0~~

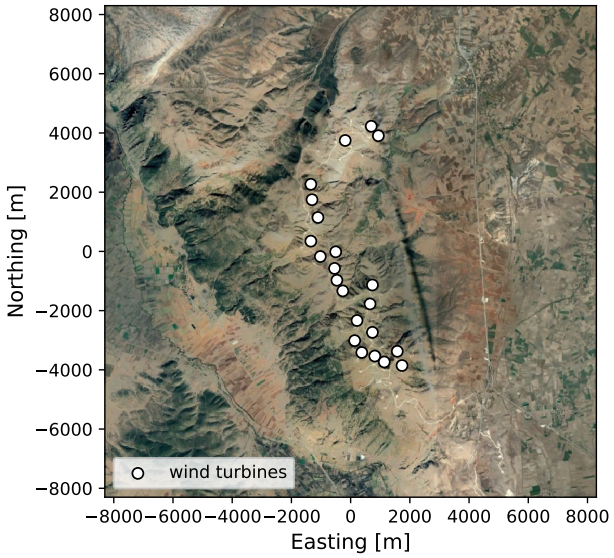

Figure 12. ~~Google Earth~~ The aerial image of the Turkish site~~. A 4 km radius circle illustrates the extent of the wind farm~~

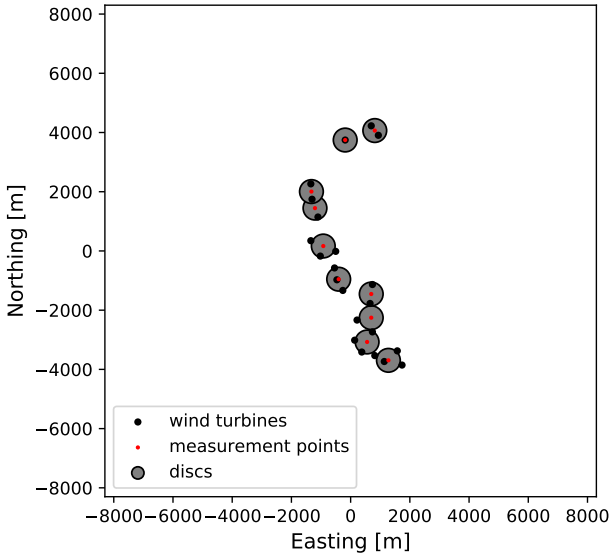

Figure 13. Measurement locations for the Turkish site: black dots - wind turbine positions, red circles - discs covering wind turbine positions, green dots - optimized measurement positions (i.e., discs' centers)

1551.0 False False7 6 696.0 -1454.0 1633.0 True True8 2 -1204.0 1446.0 1687.0 True True9 1 -1324.0 2006.0 1734.0 True True10 -184.0 3746.0 1643.0 False False

Like for the Italian site case there are only a few locations for placing the two lidars, especially for two inter-dependent reasons one being the wind farm length (8 km) and second being the average range (3 km). Once again the best solution is to place the lidars in the middle of the wind farm. The top image of Figure 14 shows the first lidar placement, which coordinates are -1900 m, -800 m and 1497 m in Northing, Easting and height asl. respectively relative to the map center coordinates (Easting 249626 m and Northing 4227308 m, UTM zone 36 S).

Knowing the first lidar position leads us to the creation of the IA GIS layers which is used for the generation of the second lidar placement layers. From the bottom image in Figure 14 there is only a narrow area in the middle of the wind farm where the second lidar can could be placed. Also, the bottom image in Figure 14 shows the result of our choice for the second lidar placement (second lidar coordinates are -400 m, -300 m and 1569 m in Northing, Easting and height asl. relative to the map center).

The designed WindScanner layout can provide measurements in 6 out of 10 measurement points which cover the middle part of the wind farm (Figure 15). The upper and lower quarter of the wind farm area are not reachable with the current layout. In principle, we would probably need two WindScanner systems to cover the entire wind farm (i.e., four scanning lidars). Considering the WindScanners and measurement locations together with the kinematic limits as the input for the last phase of the workflow we reach the optimized trajectory which total time is 16 s of which 6 s are spent on the wind speed measurements(see Table ?? and ??). This trajectory would provide us with about 35 samples of each measurement point within a 10-min period.

Angular positions for WindScanners for the Turkish site. All values rounded to two decimals. Trajectory θ_{ws1} $^\circ$ φ_{ws1} $^\circ$ θ_{ws2} $^\circ$ φ_{ws2} $^\circ$ points 1 11.6 4.83 338.16 3.82 17.22 4.74 335.27 3.513 45.3 4.91 311.65 3.354 95.88 4.6 180.35 3.855 119.25 3.54 150.71 2.736 104.14 3.01 136.48 2.3

Result of applying elevator kinematic problem on trajectory points for the Turkish site: step-stare order - indicate motion from one to another trajectory point ,$\Delta\theta_{ws}$ - angular displacement in azimuth angle (θ), ΔT_{ws} - minimum required time to complete the angular motion. All values rounded to two decimals. Trajectory order $\Delta\theta_{ws1}$ $^\circ$ ΔT_{ws1} ms $\Delta\theta_{ws2}$ $^\circ$ $\Delta T_{ws2}[ms]$ Max(ΔT_{ws1},ΔT_{ws2}) s1->2 5.62 474 2.89 340 4742->3 28.08 1110 23.63 972 11103->4 50.58 1522 131.3 3142 31424->5 23.38 967 29.64 1139 11395->6 15.11 777 14.24 755 7776->1 92.54 2374 158.31 3666 3666

4 Discussion

4.1 Discussing results

The primary purpose of the Python script described workflow and corresponding CPT tool up to date is to design a measurement campaign for wind resource assessment (WRA) using a long-range WindScanner system (Vasiljevic et al., 2016) configured in a dual-Doppler mode. This scope follows the RECAST project ambition which is focused on developing a new way of measuring the wind over a site for resource assessment, based on multiple measurement points using WindScanners. This has

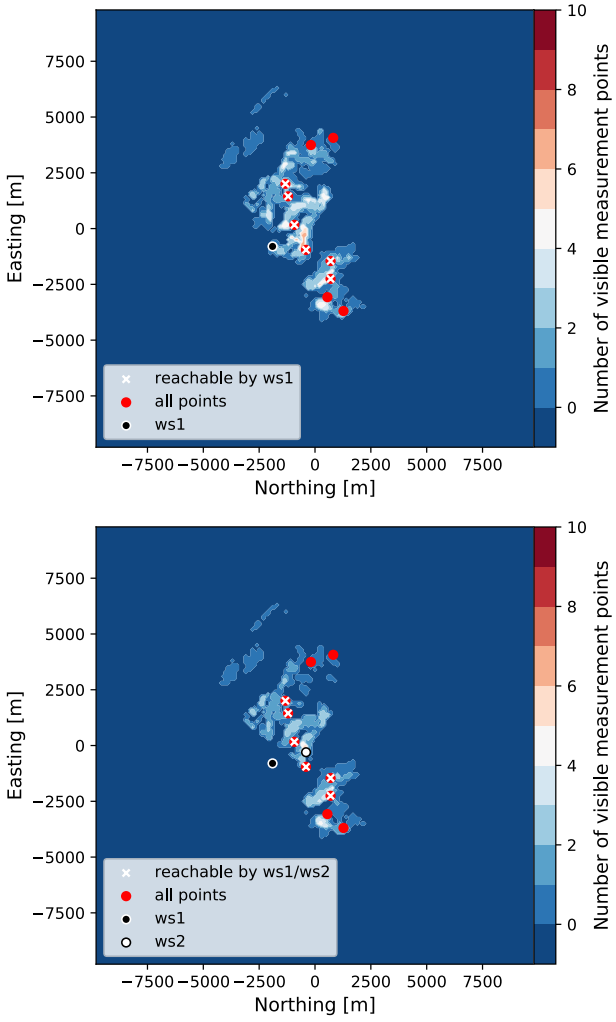

Figure 14. Placing lidars at the Turkish site: top image - locating first lidat at the ~~CB~~ combined layer, bottom image - locating second lidar at ~~IA~~ the second lidar placement layer

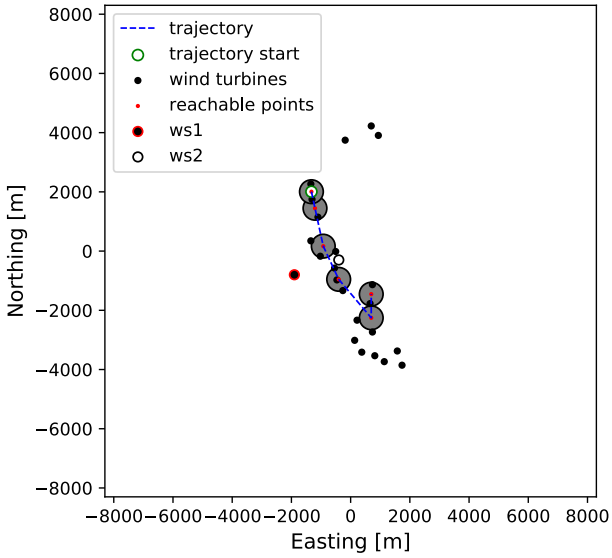

Figure 15. Final campaign layout for Turkish site

driven the choice of examples for Section 3 of this paper. However, the ~~Campaign Planning Tool~~ workflow and CPT described in this paper ~~is~~ are not limited to only planning WRA campaigns. It can be used to design any campaign using one or several scanning lidars. It can easily be applied to any type of scanning lidars since it only requires lidar specifications, which are maximum lidar range and scanner head kinematic limits (i.e., maximum ~~speed and~~ acceleration).

Planning the measurement campaign thoroughly especially with such complex instruments as scanning lidars ensures higher data availability during the campaign and eventually saves time and money. Lidars are very mobile and allow agile measurement campaigns compared to a met mast, but too often the ease of deployment is mistaken with a limited (underestimated) need of planning. This study and the CPT, in general, show the main constraints to lidar measurements in complex terrain and give a practical solution by providing the most suitable positions where the lidar can be placed.

The point of this tool is also to carefully consider the relevance or value of using scanning lidars for a measurement campaign. In the example of the Scottish site, it is relevant to question how much improvement measuring at all turbine positions makes for such a small wind farm. Is it worth using a WindScanner system instead or in addition to one met mast if we compare costs versus uncertainty in horizontal and vertical extrapolation? One way to trade off for costs is to use scanning lidars for a short period, less than the 12 months required by best practices. The challenge then is the long term correction of the measurement and the related uncertainty.

This study has shown that, for a large site like the Italian or Turkish examples, one set of two WindScanners cannot measure over the whole wind farm area. This is very important to realize at the campaign planning stage when there is still time to either give priority to one part of the site or consider using a second set of two WindScanners to cover the rest of the site.

Another major constraint that must be considered before the lidars deployment is the access roads to or near the lidar locations and possible access to a power source (e.g. existing houses, wind turbines). This is the purpose of the Satellite image used as background for the various GIS layer produced by the CPT.

In order to get around those very strong constraints, as already mentioned, it is, in any case, recommended to generate several campaign designs and to make a site visit with thorough inspection of the possible lidar positions and verification that the data used in the CPT were accurate and up to date (e.g. obstacles, tree height).

4.2 Improving workflow

The presented workflow and developed tool (CPT) can already solve many important challenges regarding the scanning lidar deployment. Nevertheless, we envisage the development of several additional modules which will improve the workflow and the developed tool.

In the current application of CPT, we were predicting the lidar range based on our experience. We plan to extend the 'Lidar range' module to be able to predict the lidar range by developing a lidar simulator. The lidar simulator will take inputs from external databases of global atmospheric visibility or aerosol optical depth for a given site and predict the expected lidar range. In mean time, our suggestion when planning the lidar campaign is to generate campaign layouts considering a conservative approach in which the expected range of the lidar should be in the range between 75 % to 50 % of the claimed range by the lidar manufacturers.

Directly connected to the range prediction is the development of a module which will predict the lidar data availability at any desired range during the planned measurement period. This module will take inputs such as the predicted range from the Lidar range module as well as the cloud height, fog or mist occurrence from the WRF model to predict the data availability.

Furthermore, the module for optimizing measurement positions will be extended by considering other criteria for finding measurement positions apart from the representativeness radius. These are for example terrain elevation, speed-up factors, roughness changes, local obstacles, etc. In principle, we will strive to incorporate anything that can cause local changes in the flow. In other words, the optimization of measurement positions will consider drivers of flow model uncertainty when finding measurement positions.

Finally, we intend to develop an eye safety module that will produce yet another restriction zone (GIS) layer for the placement of lidars. The module will impose geometrical limitations when designing campaign layout to avoid that the laser beam is steered over the site at a height where we could expect that the human eyes can be directly exposed to it.

5 Conclusions

In this paper, we have provided an exhaustive description of the workflow we recommend for planning measurement campaigns using scanning lidars or WindScanner systems. The purpose is to find the most suitable positions for the lidars given the measurement positions, the characteristics of the site (topography), the characteristics of the lidars (measurement range, kinematic limits) and the position of the two lidars relative to each other. The workflow is available through a Python library,

named the Campaign Planning Tool, which will be made public during the RECAST project. The CPT has been demonstrated for planning campaigns for resource assessment on three different sites. For a small wind farm layout, the WindScanners could be placed so that measurements could be made at all turbine positions. For the other sites, that were larger, the number of measurement points was needed to be optimized and a set of two lidars could only cover some part of the site. In any case, it is recommended to generate several possible campaign layouts and to make a site visit to take the final decision.

The CPT is easy and fast and helps to design realistic lidar measurement campaigns. Measurement campaigns are costly and risky, especially when using advanced measurement technology. The CPT helps to avoid many pitfalls that can be predicted before the start of the campaign, limiting the risks to the campaign itself.

Data availability. Data described in Section 3 of the paper are available as a data collection at https://doi.org/10.11583/DTU.c.4559624.v1

Author contributions. Conceptualization, N.V., A.V., A.B. and R.W.; Methodology, N.V. and A.V.; Software, N.V. and A.V.; Validation, N.V.; Formal Analysis, N.V.; Investigation, N.V. and A.V.; Resources, N.V. and A.B.; Data Curation, N.V.; Writing - Original Draft, N.V., A.B., R.W. and A.V.;Writing - Review & Editing, N.V., A.B., R.W. and A.V; Visualization, N.V.; Project Administration, R.W. and N.V.; Funding Acquisition, R.W. and A.B.

Competing interests. Authors declare no competing interests.

Acknowledgements. The authors would like to acknowledge Morten Thøgersen (EMD) for his support during the conceptualization phase of the study described in the paper. The financial support for the study has been provided by the RECAST project, which is funded by Innovation Fund Denmark (7046-00021B).

References

Al-Sharif, L.: Intermediate Elevator Kinematics and Preferred Numbers (METE III), Lift Report, 40, 20–31, https://www.researchgate.net/publication/275408222_Intermediate_Elevator_Kinematics_and_Preferred_Numbers_METE_III, 2014.

Bingöl, F., Mann, J., and Foussekis, D.: Conically scanning lidar error in complex terrain, Meteorologische Zeitschrift, 18, 189–195, 2009.

Biniaz, A., Liu, P., Maheshwari, A., and Smid, M.: Approximation Algorithms for the Unit Disk Cover Problem in 2D and 3D, Comput. Geom. Theory Appl., 60, 8–18, https://doi.org/10.1016/j.comgeo.2016.04.002, https://doi.org/10.1016/j.comgeo.2016.04.002, 2017.

Carta, J. A., Velázquez, S., and Cabrera, P.: A review of measure-correlate-predict (MCP) methods used to estimate long-term wind characteristics at a target site, 27, 362–400, https://doi.org/10.1016/j.rser.2013.07.004, https://linkinghub.elsevier.com/retrieve/pii/S1364032113004498, 2013.

Davies-Jones, R. P.: Dual-Doppler Radar Coverage Area as a Function of Measurement Accuracy and Spatial Resolution, Journal of Applied Meteorology, 18, 1229–1233, https://doi.org/10.1175/1520-0450-18.9.1229, 1979.

Farr, T. G., Rosen, P. A., Caro, E., Crippen, R., Duren, R., Hensley, S., Kobrick, M., Paller, M., Rodriguez, E., Roth, L., Seal, D., Shaffer, S., Shimada, J., Umland, J., Werner, M., Oskin, M., Burbank, D., and Alsdorf, D.: The Shuttle Radar Topography Mission, Reviews of Geophysics, 45, https://doi.org/10.1029/2005RG000183, https://agupubs.onlinelibrary.wiley.com/doi/abs/10.1029/2005RG000183, 2007.

Fernando, H., Mann, J., Palma, J., Lundquist, J., Barthelmie, R., BeloPereira, M., Brown, W., Chow, F., Gerz, T., Hocut, C., Klein, P., Leo, L., Matos, J., Oncley, S., Pryor, S., Bariteau, L., Bell, T., Bodini, N., Carney, M., Courtney, M., Creegan, E., Dimitrova, R., Gomes, S., Hagen, M., Hyde, J., Kigle, S., Krishnamurthy, R., Lopes, J., Mazzaro, L., Neher, J., Menke, R., Murphy, P., Oswald, L., Otarola-Bustos, S., Pattantyus, A., Rodrigues, C. V., Schady, A., Sirin, N., Spuler, S., Svensson, E., Tomaszewski, J., Turner, D., van Veen, L., Vasiljević, N., Vassallo, D., Voss, S., Wildmann, N., and Wang, Y.: The Perdigão: Peering into Microscale Details of Mountain Winds, Bulletin of the American Meteorological Society, 0, null, https://doi.org/10.1175/BAMS-D-17-0227.1, https://doi.org/10.1175/BAMS-D-17-0227.1, 2019.

Ghasemalizadeh, H. and Razzazi, M.: An Improved Approximation Algorithm for the Most Points Covering Problem, Theory of Computing Systems, 50, 545–558, https://doi.org/10.1007/s00224-011-9353-4, https://doi.org/10.1007/s00224-011-9353-4, 2012.

Izraelevitz, D.: A Fast Algorithm for Approximate Viewshed Computation, Photogrammetric Engineering Remote Sensing, 69, https://doi.org/10.14358/PERS.69.7.767, 2003.

Krishnamurthy, R., Choukulkar, A., Calhoun, R., Fine, J., Oliver, A., and Barr, K.: Coherent Doppler lidar for wind farm characterization, Wind Energy, 16, 189–206, https://doi.org/10.1002/we.539, https://onlinelibrary.wiley.com/doi/abs/10.1002/we.539, 2013.

Langreder, W. and Mercan, B.: Roaming Remote Sensing - Quantification of Seasonal Bias, in: WindEurope Summit 2016, WindEurope, https://windeurope.org/summit2016/conference/proceedings-Pr0cghyDVy/statscounter2.php?id=2&IDABSTRACT=207, 2016.

Mann, J., Angelou, N., Arnqvist, J., Callies, D., Cantero, E., Arroyo, R., Courtney, M., Cuxart, J., Dellwik, E., Gottschall, J., Ivanell, S., Kuhn, P., Lea, G., Matos, C., Palma, J., Pauscher, L., Peña, A., Rodrigo, J., Söderberg, S., Vasiljevic, N., and Rodrigues, C.: Complex terrain experiments in the New European Wind Atlas, Philosophical Transactions of the Royal Society A: Mathematical, Physical and Engineering Sciences, 375, https://doi.org/10.1098/rsta.2016.0101, 2017.

MEASNET: MEASNET Procedure: Evaluation of Site-Specific Wind Conditions, Version 2, http://www.measnet.com/wp-content/uploads/2016/05/Measnet_SiteAssessment_V2.0.pdf, 2016.

Mortensen, N., Heathfield, D., Rathmann, O., and Nielsen, M.: Wind Atlas Analysis and Application Program: WAsP 11 Help Facility, 2014.

Reinelt, G.: The Traveling Salesman: Computational Solutions for TSP Applications, Springer-Verlag, Berlin, Heidelberg, 1994.

Stawiarski, C., Träumner, K., Knigge, C., and Calhoun, R.: Scopes and Challenges of Dual-Doppler Lidar Wind Measurements—An Error Analysis, Journal of Atmospheric and Oceanic Technology, 30, 2044–2062, https://doi.org/10.1175/JTECH-D-12-00244.1, 2013.

Vasiljevic, N.: (2.5 + 5.8) Years of successes and failures with long-range WindScanner system, https://doi.org/10.5281/zenodo.1442592, https://doi.org/10.5281/zenodo.1442592, 2018.

Vasiljevic, N. and Bechmann, A.: Dual-Doppler measurement campaign design for complex terrain site in Scotland, https://doi.org/10.11583/DTU.8344028.v1, last access: 2019-07-2, 2019a.

Vasiljevic, N. and Bechmann, A.: Dual-Doppler measurement campaign design for complex terrain site in Italy, https://doi.org/10.11583/DTU.8343989.v1, last access: 2019-07-2, 2019b.

Vasiljevic, N. and Bechmann, A.: Dual-Doppler measurement campaign design for complex terrain site in Turkey, https://doi.org/10.11583/DTU.8344061.v1, last access: 2019-07-2, 2019c.

Vasiljevic, N. and Courtney, M.: Accuracy of dual-Doppler lidar retrievals of near- shore winds, https://doi.org/10.5281/zenodo.1441178, https://doi.org/10.5281/zenodo.1441178, 2017.

Vasiljevic, N. and Hasager, C. B.: WindScanner Information System, https://doi.org/10.5281/zenodo.1175211, https://doi.org/10.5281/zenodo.1175211, 2015.

Vasiljevic, N., Lea, G., Courtney, M., Cariou, J.-P., Mann, J., and Mikkelsen, T.: Long-Range WindScanner System, Remote Sensing, 8, https://doi.org/10.3390/rs8110896, http://www.mdpi.com/2072-4292/8/11/896, 2016.

Vasiljević, N., L. M. Palma, J. M., Angelou, N., Carlos Matos, J., Menke, R., Lea, G., Mann, J., Courtney, M., Frölen Ribeiro, L., and M. G. C. Gomes, V. M.: Perdigão 2015: methodology for atmospheric multi-Doppler lidar experiments, Atmospheric Measurement Techniques, 10, 3463–3483, https://doi.org/10.5194/amt-10-3463-2017, https://www.atmos-meas-tech.net/10/3463/2017/, 2017.

Vasiljevic, N., Bechmann, A., Vignaroli, A., and Wagner, R.: Campaign Planning Tool results for three sites in complex terrain, https://doi.org/10.11583/DTU.c.4559624.v2, last access: 2019-07-2, 2019.